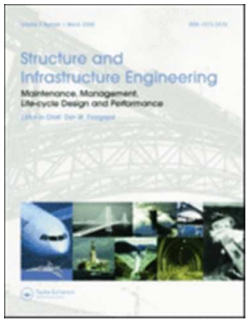

A multi-level strategy for successively improved structural analysis of existing concrete bridges: examination using a prestressed concrete bridge tested to failure

Journal:	*Structure and Infrastructure Engineering*
Manuscript ID	NSIE-2018-0112.R1
Manuscript Type:	Original Paper
Date Submitted by the Author:	29-Apr-2018
Complete List of Authors:	Bagge, Niklas; WSP Sverige AB, Department of Bridge & Hydraulic Design; Luleå University of Technology, Department of Civil, Environmental and Natural Resources Engineering Plos, Mario; Chalmers Univeristy of Technology, Department of Civil and Environmental Engineering Popescu, Cosmin; Northern Research Institute, ; Luleå University of Technology, Department of Civil, Environmental and Natural Resources Engineering
Keywords:	Bridges, Codes, Nonlinear analysis, Assessment, Concrete, prestressed, Shear strength, Structural behavior, Finite element method, Bridge failure, Bridge tests

Note: The following files were submitted by the author for peer review, but cannot be converted to PDF. You must view these files (e.g. movies) online.

NSIE-2018-0112.R1-tables-figures.zip

A multi-level strategy for successively improved structural analysis of existing concrete bridges: examination using a prestressed concrete bridge tested to failure

Niklas Bagge[1,4*], Mario Plos[2], Cosmin Popescu[3,4]

[1]*Department of Bridge & Hydraulic Design, WSP Sverige AB, Ullevigatan 19, 411 40 Gothenburg, Sweden, Phone: +46 10 722 92 71, E-mail: niklas.bagge@wsp.com, ORCID: 0000-0001-8889-4237*

[2]*Department of Civil and Environmental Engineering, Chalmers University of Technology, 412 96 Gothenburg, Sweden, Phone: +46 31 772 22 44, E-mail: mario.plos@cth.se, ORCID: 0000-0002-2772-9120*

[3]*Norut Northern Research Institute, Rombaksveien E6-47, 8504 Narvik, Norway, +46 920 49 23 22, E-mail cosmin.popescu@norut.no, ORCID: 0000-0001-9423-7436*

[4]*Department of Civil, Environmental and Natural Resources Engineering, Luleå University of Technology, Luleå.*

*Corresponding author

Abstract

This paper describes a multi-level strategy with increased complexity through four levels of structural analysis of concrete bridges. The concept was developed to provide a procedure that supports enhanced assessments with better understanding of the structure and more precise predictions of the load-carrying capacity. In order to demonstrate and examine the multi-level strategy, a continuous multi-span prestressed concrete girder bridge, tested until shear failure, was investigated. Calculations of the load-carrying capacity at the initial level of the multi-level strategy consistently resulted in underestimated capacities, with the predicted load ranging from 25 % to 78 % of the tested failure load, depending on the local resistance model applied. The initial assessment was also associated with issues of localising the shear failure accurately and, consequently, refined structural analysis at enhanced level was recommended. Enhanced assessment using nonlinear finite element (FE) analysis precisely reproduced the behaviour observed in the experimental test, capturing the actual failure mechanism and the load-carrying capacity with less than 4 % deviation to the test. Thus, the enhanced level of assessment, using the proposed multi-level strategy, can be considered to be accurate, but the study also shows the importance of using guidelines for nonlinear FE analysis and bridge-specific information.

Keywords: bridges; codes; full-scale failure test; nonlinear finite element analysis; modelling strategy; multi-level assessment; prestressed concrete; shear capacity; structural behaviour.

1 Introduction

For the development of sustainable management of bridges, optimised strategies are required to meet current and future demands. Bridges are ageing, whilst their structures are deteriorating and traffic intensities, speeds and loads are continually increasing. This has resulted in a greater need for assessment, inspection, monitoring, repair, strengthening, replacement and tools to help produce optimal solutions. For instance, in European countries, there is a need to strengthen 1500 bridges, and replace 4500 bridges and 3000 bridge decks out of approximately 276 000 railway bridges (MAINLINE 2013). Moreover, of the 608 000 highway bridges across the United States, 10.5 % are classified as structurally deficient and

13.9 % are considered to be functionally obsolete (U.S. Department of Transportation 2016). These issues have also been highlighted in research projects reported in BRIME (2001), COST-345 (2004), SAMARIS (2006) and SB (2007b). There are, therefore, a vast number of bridges to be assessed with limited resources.

In the pursuit of systematic assessments of existing bridges, general bridge assessment approaches have been proposed, for instance, in SB (2007a), UIC 778-4R (2009), ISO 2394 (2015) and Schneider and Vrouwenvelder (2017). All these approaches follow a principle of gradual improvement of the assessment, and different assessment levels have been defined depending on the complexity of the methods involved. Based on the same principle, the flow chart in Figure 1 illustrates a general assessment approach for existing bridges. When a bridge assessment is necessary, possibly due to the requirements of the structure being changed (e.g. increased loads), deterioration or damage (e.g. reinforcement corrosion, frost damage or alkali-silica reaction) or due to reconstruction, the bridge is initially analysed using simplified methods. At this stage, the assessment is carried out based on similar methods to those used to design the structure, using available information about the bridge. Where the assessment requirements are not fulfilled at the initial stage, the next step is to identify the different options available, either leading to the bridge being kept in service or demolished and replaced.

Based on the current state of the structure, the goal is to find the optimal sustainable solution in a life cycle analysis. As economic, societal, and environmental aspects have to be considered, all with regard to an acceptable level of safety for the user, a risk evaluation of available options has to be carried out (Ellingwood & Lee 2016; Frangopol & Soliman 2016). The decision on how to proceed should then be supported by the weighted value (often a monetary value) given through risk analysis including the aspects mentioned above (Bocchini et al. 2013). Available options to consider, if the initial assessment does not fulfil the actual requirements on the bridge, can be categorised as: (1) enhanced assessment, (2) redefined use of the bridge, (3) intensified inspection and monitoring, (4) repair or strengthening or (5) demolition and replacement. In the enhanced assessment, improvements can be grouped as being informative or analytical. Inspections, monitoring, evaluation of site-specific loads and testing (e.g.,

material testing and proof loading) can be considered as providing improved information for model updating. Improved analysis can be accomplished by refined structural analysis, models estimating the local resistance and by refined safety verification (e.g., probabilistic analysis). With risk-based decision-making as the driving force in the assessment, an assessment approach, with increasing levels of complexity, is recommended and, if shown to be necessary, several successive steps at the enhanced level may be needed to meet the requirements. In contrast to the design of new bridges, more detailed information about the actual structure can be taken into account in the evaluation of existing bridges. In order to provide precise and reliable assessments, such information, reducing the uncertainties associated with materials, geometries, boundary conditions and loads, plays an important role.

Structural analysis and verification of action effects are essential parts of the structural assessment. The procedure to carry out structural analysis is widely described in the literature, with the finite element method (FEM) being an important tool. In practice, linear finite element (FE) analysis is most commonly used, for which recommendations for use with concrete structures are provided, for instance, by fib (2008), Rombach (2011), and Pacoste et al. (2012). In order to estimate the structural behaviour more precisely, nonlinear FE analysis can be used. With a more accurate representation of material and structural responses, this type of FE analysis is regarded as having the best potential for accurate prediction of the load-carrying capacity (SB-LRA 2007). Some examples where nonlinear FE analysis has been used to determine the capacity of existing RC bridges are reported by Huria et al. (1993), Plos (2002), Song, You, Byun and Maekawa (2002), Plos and Gylltoft (2006), Broo et al. (2007), Schlune (2011), Puurula et al. (2015), and Šomodíková et al. (2016).

However, this kind of analysis is complex, and comparison of the procedures for the modelling in these studies reveals significant variations. Within the nonlinear FE analysis (also valid for linear FE analysis), assumptions associated with geometry, boundary conditions, constitutive material models and solution methods are necessary and the outcomes from the analyses are highly dependent on the modelling choices; these, in turn, rely on the analyst's knowledge and experience (Belletti et al. 2013). The variation in outcomes from analysis of one single structure with numerous different assumptions

made by different engineers can, however, be reduced by applying modelling instructions based on current technical knowledge. At present, nonlinear FE analyses are used daily within the research community but, in order to make such methods practically applicable, more robust and more reliable for practicing engineers, guidelines with such instructions are needed. Attempts to provide general guidance for nonlinear FE analysis of concrete structures have been presented by Broo et al. (2008), fib (2008) and Hendriks et al. (2017). Targeting specific software, recommendations are also provided by, for instance, ABAQUS (2012), ANSYS (2013), ATENA (2016b) and DIANA (2015). Nonetheless, in order not to limit the analysis to a specific piece of software, guidelines developed for bridge assessment should be based on the available, and in the research community well-established and accepted, modelling choices.

Due to the complexity of bridge assessment and the high computational demands of nonlinear FE analyses, the structural analysis and the verification of action effects should be successively improved. Despite this, limited detailed guidelines exist on how this successive increase in complexity should be carried out for bridges. In the assessment approach shown in Figure 1, it is mostly described in general terms. Recently, such guidelines, describing different modelling choices, have been proposed by Plos et al. (2017) for assessing the load-carrying capacity of concrete (bridge deck) slabs at several levels of complexity. In our work, a strategy for the structural analysis of bridge superstructures, including systems of beams and slabs, has been formulated, thus extending the previous strategy. As with the general assessment approach (see Figure 1), the structural analysis strategy includes a progressively more accurate representation of the real structural behaviour. The ultimate goal is to provide engineers with a framework which facilitates a more efficient assessment of existing bridges.

In order to validate various methods of bridge assessment, a prestressed concrete (PC) girder bridge was subjected to a variety of experiments, such as a test to structural failure (Bagge et al. 2014). As accurately determining the shear capacity of concrete structures is difficult, and the subject of much debate in the research community, the failure test was particularly focused on shear-related failure modes. Furthermore, only a few reinforced concrete (RC) bridges have been investigated with regard to shear-related failures, with research limited to the studies reported by Burdette and Goodpasture (1971), Weder

(1977), Pedersen et al. (1980), Plos et al. (1990), Aktan et al. (1992), Azizinamini et al. (1994), Isaksen et al. (1998), Haritos et al. (2000), Pressley et al. (2004) and Puurula et al. (2015). The outcomes from these studies have also been summarised and further discussed in Bagge et al. (2018). Apart from a better understanding of the shear behaviour of full-scale concrete bridges, the primary advantage of the rare information given by this additional failure test is that it assists in examining the efficacy of the proposed strategy for structural analysis. The paper also contributes by evaluating the validity and applicability of guidelines for nonlinear FE analysis applied to bridge assessment. Herein, the general guidelines provided by Hendriks et al. (2017) were investigated, since they are the most precise in terms of recommendations, while work by Broo et al. (2008) and fib (2008) is more informative regarding issues relating to such analysis of RC structures.

In this study, the commercial software ATENA Studio (ATENA 2016b) was used and, consequently, both the general guidelines and the software-related recommendations were treated in combination. This is a highly relevant study given the lack of studies of the guidelines in relation to full-scale structures. Previously, the recommendations have been shown to work rather well for small-scale laboratory experiments (Belletti et al. 2013) but their suitability for the assessment of full-scale *in situ* bridges was untested. For instance, issues relating to computational effort become more relevant for larger structures. The examination of the guidelines for nonlinear FE analysis and also the proposed strategy for structural analysis should be seen as an ongoing task seeking to confirm their practicality. A complete verification for every scenario cannot be achieved for this kind of problem (Oreskes et al. 1994); however, this study can be beneficial for more precise and reliable bridge assessments in the future.

2 Multi-level strategy for structural analysis

It is proposed that the structural evaluation in the enhanced assessment (see Figure 1) follows a multi-level procedure, with a gradually increasing complexity of the analysis. The new proposal is visualised in Figure 2. Thus, a more thorough consideration of the structural response and load-carrying capacity can

be obtained. This concept of gradually increasing the complexity of the analysis was developed particularly for the ultimate limit state, and is an extension of the strategy described for concrete slabs by Plos et al. (2017). The updated strategy provides a more complete approach for structural analysis of bridge superstructures consisting of systems of concrete beams and slabs. Based on the types of failures covered by the structural analysis, different complexities of analysis can be defined. At the initial level (Level 1), only action effects are calculated in the structural analysis, so an additional verification using resistance models to verify the cross-sectional capacity is required. In contrast, the highest level (Level 4) is a one-step procedure where the analysis implicitly determines the capacity with regard to possible failure modes that can occur. In this strategy, the failure modes identified are related to flexure, shear or anchorage, and are gradually included in the structural analysis from Level 2 to the complete analysis at Level 4. Here, shear types of failures, including punching and torsion, are taken into account along with, in the presence of axial forces, the combination of those forces and flexure moments.

The methods associated with the initial level (Level 1) are referred to as current, or traditional, approaches for structural analysis (i.e., no failure modes are reflected in the structural analysis) and the subsequent levels (Levels 2 to 4) are referred to as enhanced approaches, taking nonlinearities into account. In order to ensure sufficient capacity with regard to failure modes not implicitly reflected in the structural analysis, the calculated action effects are checked with local resistance models. For example, models are provided by the European (SS-EN 1992-1-1 2005), American (ACI 318 2014), Canadian (CSA A23.3 2014) design standards, Model Code 2010 (fib 2013) or national design regulations.

The proposed multi-level strategy does not specify which model to use. However, the general recommendation is to use resistance models that are expected to give a similar level of approximation to that of the structural analysis. In order to ensure the required margin of safety, the concept used for safety verification also has to remain consistent with the level of assessment and structural analysis. Moreover, better information about material properties, the geometry of the bridge, boundary conditions and loading is recommended as the level of structural analysis increases. With a deteriorating structure, the impact of such deterioration should be taken into account with this information. This means that both the

information and the analysis in the enhanced assessment is more complex, as shown by the assessment approach in Figure 1. In the proposed strategy, the level of idealisation in terms of number of dimensions (2D or 3D) is not restricted. Actually, either 2D or 3D can be assumed at each level of analysis, as long as the structural model appropriately handles the aspects being assessed.

2.1 Level 1 – Structural analysis of action effects

At the initial level, standard methods are used to calculate the distribution of internal forces and moments for certain combinations of loads. In the next step, the associated local resistance is determined and compared to the action effects in order to verify the load-carrying capacity. Typically, the theory of linear elasticity is applied in the structural analysis at both serviceability and ultimate limit states (Level 1A). However, in the case of statically indeterminate structures (e.g., slabs and continuous beams), Level 1 can be extended to two sub-levels, covering the load-carrying capacity of sections not fully dealt with by linear elastic analysis. The analysis at Level 1B uses the theory of elasticity but allows limited redistribution of internal forces and moments based on empirical findings and, at Level 1C, the plasticity theory is used with verification of the rotational capacity (CEB 1998). Thus, the proposed strategy for structural analysis is consistent with the four levels of idealisation stated in Model Code 2010 (fib 2013), in which the nonlinear methods, here used at Levels 2 to 4, comprise the last idealisation.

Apart from other methods at this level, the FE method, assuming a linear response, is a powerful tool to determine the distribution of action effects in the structure and compare them to associated sectional resistance. Moreover, the method allows the handling of a large number of load combinations in a rational way. The concept of FE modelling for investigation of RC structures is, for instance, described in fib (2008), Pacoste et al. (2012) and Rombach (2011). Typically, structural finite elements (beam and/or shell) are used to represent the actual geometry of the bridge.

2.2 Level 2 – Structural analysis accounting for flexural failures

The next step of the multi-level strategy for structural analysis is to account for the nonlinear structural behaviour, mostly associated with material nonlinearities but also, in some cases, geometric nonlinearities

(fib 2008). In contrast to the previous level of approximation, the analysis should preferably be limited to specific loading situations shown to be critical earlier in the assessment. Incrementally increasing the load applied to the structure, the structural behaviour and, ultimately, the failure determined by the model can be examined.

The analysis at Level 2, as well as the higher levels following the enhanced approach, is preferably carried out using the FE method. The same finite element types used at the previous level, but updated with nonlinear properties, can be applied. For a 3D model, the following representation of structural element types can be used: (1) beams and columns modelled with beam elements, and (2) walls and slabs modelled with shell elements. Here, there are also situations where several structural elements can be combined into beam elements (e.g., a bridge deck slab and beam into a single beam element). The reinforcement is included in the model in its actual position, simplified by modelling a perfect bond without any slip between the reinforcement and the surrounding concrete, either embedded in the element or as individual elements.

In general, beam elements cannot take into account shear types of failure with sufficient precision, and no out-of-plane shear failures are accounted for by shell elements. However, although nonlinear flexural behaviour can be accounted for using elastic analysis with limited redistribution and plastic analysis at Level 1, this Level 2 model treats such nonlinearities more accurately. Thus, out-of-plane shear-related failures and anchorage failures are not accounted for in the structural model and need to be checked separately using the appropriate resistance models.

2.3 Level 3 – Structural analysis accounting for flexural and shear-related failures

In addition to the flexural behaviour, the aim of the nonlinear analysis at Level 3 is to account for relevant shear-related failures. With an FE model, this can be accomplished by using element types that allow the shear response to be calculated. Beam elements need to be updated to be either shell or continuum elements, depending on the presence of out-of-plane shear. Similarly, shell elements need to be changed to continuum elements if out-of-plane shear is to be modelled. There are beam elements developed to

account for the shear response, see Mohr et al. (2010) and Ferreira et al. (2015). Nevertheless, such elements should be carefully used, since the shear-related failure modes are not necessarily captured accurately by these elements. Again, the reinforcement is modelled with a perfect bond to the surrounding concrete using embedded or individual reinforcement elements. Thus, anchorage failure is the only main type of failure not taken into account by the structural analysis and needs to be explicitly checked using separate resistance models.

2.4 Level 4 – Structural analysis accounting for flexural, shear-related and anchorage failures

At Level 4, a similar configuration of finite elements can be used as for the previous levels. In addition, an interface model describing the bond-slip behaviour between the reinforcement and the concrete needs to be implemented to enable implicit verification of anchorage failures. Such an implementation means that all major failure modes can be checked directly in the structural model. To simulate bond-slip behaviour, the reinforcement normally needs to be modelled using separate elements and are not embedded in the shell or continuum elements representing the concrete. Usually, reinforcement bars are idealised with 1D truss elements. The anchorage capacity can also be taken into account with different detailing. Such an approach for successively improved analysis of the anchorage capacity has been proposed by Tahershamsi et al. (2017), and this can be incorporated in the multi-level structural assessment strategy.

3 *In situ* bridge test

3.1 General description

In order to evaluate and improve the methods of assessing the load-carrying capacity of existing concrete bridges, a PC bridge has been extensively investigated including the loading of several structural elements to failure. The test was carried out in 2014 on a 55 year-old viaduct across the E10 road and the railway yard at Kiruna, Sweden. The Kiruna Bridge was built as part of the road connecting the city centre and a nearby iron ore mine. As a consequence of extensive mining-related subsidence, an urban

transformation of city was started, involving the decommissioning of the infrastructure in the region affected. Consequently, the bridge was permanently closed in October 2013 and demolished about a year later, although it was in a good condition. From inspections of the bridge, only some older cracks adjacent to the intermediate supports, assumed to have occurred during the time of construction, were identified (Bagge et al. 2015a; Enochsson et al. 2011). Moreover, no visible degradation of the non-prestressed reinforcement, or of the prestressed reinforcement, was found when the bridge was demolished.

3.2 Bridge geometry

The bridge was a continuous girder bridge with a total centre line length of 121.5 m in five spans of lengths 18.00, 20.50, 29.35, 27.15 and 26.50 m (see Figure 3). The superstructure consisted of three parallel prestressed, longitudinal girders and a 14.9 m wide connected RC deck slab, with additional curbs on each side (300 × 300 mm^2). The bridge was inclined 5.0 % longitudinally, 2.5 % transversally and the western part was curved along 84.20 m with a radius of 500 m, while the remaining 37.30 m was straight. Although the entire superstructure, according to the construction drawings, was continuously curved, inspection revealed that construction had been simplified by using straight girders between the supports.

The intermediate supports consisted of three quadratic columns (550 × 550 mm^2). In 2010, these were fitted with a pot bearing at their base to allow rotation (Bagge et al. 2015a). At the western abutment, the superstructure was supported by longitudinally and transversally restrained bearings, while longitudinal motion was free at the eastern abutment. In relation to the longitudinal axis of the bridge, supports 1 – 6 and associated foundations were rotated 100°, 100°, 108°, 92°, 99° and 99° counter-clockwise.

The girders, 5.00 m apart, were 1920 mm high including the slab, with their width being 410 mm, increasing to 650 mm at the supports over a distance of 4.00 m. Their width was 550 mm at casting joints located one quarter of the span length west of support 3 and one third of the span length east of support 4 (see Figure 3). Between the girders, the slab was 220 mm thick with a gradual increase over a distance of 1.00 m to 300 mm at the girder-slab intersection. The cantilevers were 330 mm thick at the girder-slab

intersection, 160 mm at the curbs and were 1.835 m in width. The girders were also connected with cross-beams at each support (600 × 1700 mm^2) and at the third point of each span (300 × 1400 mm^2), except in span 1 where one cross-beam connected at midspan.

A BBRV post-tensioning tendon system consisting of 32 strands with a diameter of 6 mm in grouted ducts was used to prestress the girders. First, the central segment between the casting joints was prestressed from both ends with six tendons in each girder, followed by prestressing of the segments to the west and east from the corresponding abutments using four and six tendons in each girder, respectively. The system of tendons was parabolically aligned with the lowest vertical positions at the midspans and the highest at the supports. Due to limited documentation about the bridge, the initial prestress force was unknown. In addition, each girder was reinforced longitudinally with three 16 mm diameter bars at their base, increasing to five 25 mm diameter bars at the intermediate supports 2 – 4. On the sides, the girders were reinforced with 10 mm diameter longitudinal bars with 150 mm spacing for the central girder and 200 mm for the two other girders. In the vertical direction, the girders were reinforced with 10 mm diameter double-legged, closed stirrups with a spacing of 150 mm, and a 30 mm thick concrete cover.

3.3 Material properties

Construction drawings of the bridge specified two concrete quality classes (denoted K300 and K400), implying higher strength in the superstructure than in the substructure. However, the Swedish assessment code (TDOK 2013:0267 2017) recommends upgrading the material characteristics of these classes of bridges that were designed according to the regulations between 1947 and 1960. The characteristic cylinder compressive strengths and modulus of elasticity to be used for design and assessment, respectively, are given in Table 1. In connection to the full-scale tests, 25 cores with 100 mm diameter and 200 mm height were drilled out and tested (seven from the slab, eleven from the girders and seven from the columns) to determine the *in situ* properties of the concrete. The tests were conducted in accordance with the standards SS-EN 12504-1 (2009), SS-EN 12390-3 (2009) and SS-EN 12390-13

(2013). They revealed that the type of concrete was probably the same in all structural parts of the bridge (see Table 1). Nevertheless, there was a substantial range of strengths, for instance, the coefficient of variation was 16 % for the overall concrete compressive strength with a mean value of 62.2 MPa.

In the bridge, three quality classes of reinforcing steel were used. The post-tensioned tendons were of St145/170 and the non-prestressed reinforcement was either of Ks40 or Ks60. The non-prestressed reinforcement in the girders was solely Ks40, while a mixed configuration of Ks40 and Ks60 was used in the bridge deck slab. Tensile tests have been carried out for each class and bar dimension according to the European standards SS-EN ISO 6892-1 (2009), SS-EN ISO 15630-1 (2010) and SS-EN ISO 15630-3 (2010). Together with the characteristic design and assessment values (TDOK 2013:0267 2017), mean values of the tested yield strengths (0.2 % proof strength for prestressing steel), tensile strengths and strains at peak stress are summarised in Table 2.

3.4 Experimental investigation

An experimental investigation was carried out in order to understand the behaviour of different structural parts of the bridge, thoroughly described in Bagge et al. (2014) and summarised in the following steps:

1. Non-destructive evaluation of the residual prestress tendon forces, see Bagge et al. (2017).
2. Preloading schedule 1 of the girders to investigate the overall structural behaviour and destructive evaluation of the residual prestress tendon forces, see Bagge et al. (2017).
3. Preloading schedule 2 of the girders strengthened with carbon fibre reinforcing polymers (CFRP) to investigate the strengthening effect on the structural behaviour, see Nilimaa et al. (2015) and Nilimaa (2015).
4. Failure loading of the south and central girders to determine the failure mechanism and load-carrying capacity.
5. Failure loading of the bridge deck slab to determine the shear failure mechanism and load-carrying capacity, see Bagge et al. (2015b).

Part of the experimental programme was to study two separate strengthening systems using CFRP attached to the concrete. After the first preloading schedule, the bases of the central and south girders in span 2 were fitted with three 10 × 10 mm^2 near-surface mounted (NSM) CRFP rods in 17 × 17 mm^2 sawn grooves (Nilimaa et al. 2015) and three 1.4 × 80 mm^2 prestressed CFRP laminates (Nilimaa 2015), respectively (see Figure 3). Both systems were bonded to the concrete with a thixotropic two-component epoxy adhesive. The laminates were prestressed with 100 kN, each using a temporary stressing device at the laminate ends, which also functioned as a mechanical anchor while the epoxy was curing (Nilimaa 2015). For the CFRP materials, the nominal tensile strength and modulus of elasticity was 3300 MPa and 210 GPa, respectively.

Loading the bridge girders to failure was achieved by using two steel load distribution beams simply supported centrally above the girders in the midsection of span 2 (see Figure 3). In order to arrange the beams horizontally, horizontal concrete surfaces were cast locally on the slab and complemented with load distribution steel plates (700 × 700 mm^2) on top. Using wires run through drilled holes in the bridge slab (diameter of 200 mm), anchored in the bedrock, four force-controlled hydraulic jacks loaded the superstructure. The centre-to-centre distance between each jack and the closest support of the steel beams where the load was transferred to the bridge was 885 mm.

The girder preloading sequences (i.e., steps 3 and 4 of the experimental programme summarised above) were as follows: the load delivered by the two outer jacks (Jacks 1 and 4 in Figure 3) was approximately equal to half the load produced by the inner jacks (Jacks 2 and 3), up to 6 MN (the maximum load used), followed by the unloading of the structure. This loading pattern was also followed in the failure test, up to a total load level of 12.0 MN, after which only the load in the outer jack adjacent to the south girder (Jack 1) was increased until failure of that girder. The same procedure was followed for the inner jacks (Jacks 2 and 3) until there was a structural failure of the central girder. However, due to the subsequent test of the bridge slab behaviour and its load-carrying capacity, the north girder was not further loaded to failure. The loading schedule of the failure test of the south and central is shown in Figure 4. Also shown are some virtual drops in the loads; however, these are only as a result of a new

mounting being made between the hydraulic jacks (see Figure 3) and the bedrock anchored wires to produce larger deformations than allowed by the maximal stroke length (i.e. reduced registered oil pressure in the hydraulic jack while maintaining the applied load).

A measuring programme with 140 sensors was designed to monitor the structural behaviour of the superstructure in the failure tests. The equipment installed is summarised below (see Bagge et al. (2014) for detailed description):

- **Oil pressure:** Measured with oil pressure sensors attached to each hydraulic jack (4 sensors).
- **Vertical displacement:** Measured with draw wire sensors between the base of each girder and the ground at midspans 1 – 3, and between the base of the cross-beam, adjacent to the column, and the basement at supports 2 – 3 (13 sensors).
- **Horizontal displacement:** Measured longitudinally and transversally with a Noptel displacement sensor on the cantilever slab adjacent to the south column at support 3 and longitudinally with linear displacement sensors at the base of the exterior girders at support 6 (3 sensors).
- **Crack opening:** Measured with a crack opening displacement sensor at a major crack on the south girder in the mid-region of span 2 (1 sensor).
- **Curvature:** Measured with a curvature rig having 5 linear displacement sensors placed on top of the slab above the central girder centrically at supports 2 – 3, and mounted at the base of the central girder at midspan 2 (15 sensors).
- **Concrete strain:** Measured with vertically aligned strain gauges at the base of the columns at supports 2 – 3 (24 sensors).
- **Longitudinal reinforcing steel strains:** Measured with strain gauges on three levels (base, top and intermediate) of each girder in the mid-region of span 2 and the adjacent support regions (39 sensors).

- **Vertical reinforcing steel strains:** Measured with strain gauges on three stirrups west of midspan 2 on the south girder (9 sensors).
- **CFRP rod strains:** Measured with strain gauges in the mid-region of span 2 and the overlapping zone 4.5 m west of the midspan (14 sensors).
- **CFRP laminate strains:** Measured with strain gauges in the midspan region and at the anchorage zone (10 sensors).
- **Temperatures:** Measured with temperature wires on each girder and the bridge deck slab in midspan 2 (8 wires).

The oil pressure and the concrete strains in the columns were measured to calculate the externally applied loads and estimate the reaction forces at the adjacent supports, respectively. Together with measurements of displacements and strains in the longitudinal reinforcement, these measurements were expected to capture general structural responses. In order to evaluate the performance of the strengthening systems, for instance, strains around the anchorage and overlapping zones were measured to assess their behaviour. Prior to the tests, pre-analyses of the bridge indicated that the shear capacity may be critical for the load-carrying capacity of the girders. Based on these findings, the strain measurements were carried out on the south girder. In addition, a digital image correlation (DIC) technique was used to capture displacements and strains over an area, theoretically, of 1050 × 880 mm^2. The measurements were carried out on the lower part of the south girder with the centre 2.0 m west of the midspan. The tests were also recorded using a set of video cameras.

4 Initial structural assessment

The assessment methods at Level 1 in the multi-level strategy (see Figure 2), currently used in engineering practice, were initially applied and evaluated based on the failure tests of the bridge girders. At this level, the load-carrying capacity was determined through comparison of the action effects from a structural analysis, also accounting for redistribution of internal forces, with the sectional capacity given by local resistance models. For this particular investigation of the Kiruna Bridge, anchorage failures were

not critical for the load-carrying capacity and, thus, the focus was on the flexural and shear capacity. As the theoretically estimated structural response and load-carrying capacity were to be compared, no safety margin was included in the initial assessment. Consequently, the mean values of material properties were used in the calculations.

4.1 Structural model

The structural response of the bridge was modelled using the software ATENA Studio (ATENA 2016b) based on the FE method (see Figure 5). The actual bridge geometry specified in the construction drawings was modelled with only a few simplifications. As the impact of the abutments and the surrounding soil material on the structural response for the load case studied was negligible, they were not included in the model. In the model, the following element types were used to represent the geometry: (1) shell elements (*CCIsoShellBrick*) for the bridge deck slab, the foundations and the steel plates composing the load distribution beams, (2) beam elements (*CCIsoBeamBrick*) for the girders, cross-beams, curbs and columns, (3) continuum 3D elements (*CCIsoBrick*) for the bearings and loading plates and (4) truss elements (*CCIsoTruss*) for the tendons and NSM CFRP rods installed on the central girder (prestressed CFRP laminates in the south girder were excluded due to premature debonding in the bridge test, see Section 6.1 for further information). Moreover, the non-prestressed reinforcement was modelled as embedded reinforcement in the beam and shell elements in their actual locations. In general, the size of the finite elements in the bridge model was approximately 1.0 m (i.e., along the longitudinal beam axes and along the in-plane shell axes), with further refinement of the mesh size locally at bearings and in the load distribution plates and beams. Linear elastic material properties were assigned to the elements using the following modulus of elasticity with Poisson's ratio specified in brackets: 32.1 GPa (0.15) for the concrete, 210 GPa (0.3) for the structural steel, 210 GPa for the prestressed tendons and the NSM CFRP rods and 200 GPa for the non-prestressed reinforcement.

The steel plates representing the bearings at support 1 were constrained for displacement in the vertical, transverse and longitudinal directions of the bridge, while the steel plates at support 6 allowed

displacement in the longitudinal direction. By having the constraints along a transverse line of the bearings, the superstructure was free to rotate around the transverse axis at the abutments. The foundations at the intermediate supports, at the base of the columns, were cast directly on bedrock and, thus, the bottom surface of the foundation was fixed in all directions. As a result of the joints that were installed at the bases of the columns a few years before the test (Bagge et al. 2015a), the columns were free to rotate relative to the foundation in the load sequences associated with the failure loading.

At the time the bridge was tested, the actual prestress forces in the tendons were unknown. The experimental programme therefore included attempts to determine the residual prestress forces after 55 years in service by using both destructive and non-destructive test methods, see Bagge et al. (2017). However, these *in situ* tests involved several uncertainties not fully investigated and clarified. Thus, the evaluation of the girder failure test has been based on theoretically determined values. Parameters influencing the prestress losses were taken into account, including initial losses associated with the construction and the time-dependent effects thereafter. As there was a lack of information about the initial prestress forces, the upper stress level allowed according to the design code (BBK 94 1994) was assumed, i.e., the lower of $0.85f_{p0.2k}$ (1233 MPa) and $0.75f_{tk}$ (1275 MPa) before locking the anchor device, and the lower of $0.80f_{p0.2k}$ (1160 MPa) and $0.70f_{tk}$ (1190 MPa) after locking and relaxation of the tendon.

At the construction phase, the friction losses due to intended and unintended angle changes of the ducts were accounted for by using a friction coefficient of 0.2 and a wobble friction coefficient of 0.01 rad/m according to the manufacturer of the current prestressing system (Strängbetong n.d.). In order to determine the time-dependent prestress losses, concrete shrinkage (0.25 ‰) and creep (creep coefficient of 2.0) were taken into account following the design code (BBK 94 1994), and the steel relaxation (8 % at a steel stress of $0.65f_{tk}$ and 0 % at or below $0.45f_{tk}$ with a linear interpolation between these specified values) according to the specification by the manufacturer of the prestressing system (Strängbetong n.d.).

The same loading procedure as in the failure test of the girders was followed for the theoretical assessment of the load-carrying capacity (see Figure 5b for the loading setup in the structural model). However, only the symmetric load configuration below 12 MN was applied to produce the action effects

in the superstructure. In addition to the loads produced by the hydraulic jacks, the residual prestress forces and the dead weights of the bridge and equipment utilised to apply the external loads were included in the analysis. For verification of the load-carrying capacity, the action effects (i.e. axial force, shear force and moment) were extracted in sections in span 2 with approximately 1.0 m spacing. In order to investigate the bridge using Level 1B of the multi-level strategy (see Figure 2), the FE model was also used with a plastic hinge introduced in the location where the critical moment capacity was reached.

4.2 Local resistance models

At Level 1 in the multi-level strategy, the response from the structural analysis is compared to results from the local resistance models. The capacity assessment was started with calculations of the moment and shear resistances, and localisation of the critical section based on linear elastic structural analysis. Redistribution of internal forces, from the section that reached moment capacity determined by the linear analysis, was thereafter utilised (at Level 1B of the multi-level strategy) for cases where shear capacity was not reached in the structure. Model Code 2010 (fib 2013) was used as a basis for determination of the local resistances and the available degree of moment redistribution. It was also complemented with a comparison to the shear resistance according to the European standard (SS-EN 1992-1-1 2005).

The geometry of the superstructure was simplified to three T-shaped beams for calculation of the moment resistance in the span subjected to an external load in the test. Here, the traditional standard method of effective flange widths and concrete block of uniformly distributed compressive stresses was assumed. In order to determine the load-carrying capacity of the bridge girders due to shear, the local resistance models at Levels I to III in the Model Code 2010 were used. The model at Level I, relying on the variable-angle truss model approach with limitations based on the theory of plasticity (Nielsen & Hoang 2010; Thurlimann 1979) as used for the model in the European standard, provides the simplest analysis and is expected to produce the most conservative result. The models at Levels II and III, based on a generalised stress-field approach (Bentz & Collins 2006; Bentz et al. 2006), provide greater complexity but also a higher accuracy.

5 Enhanced structural assessment

In cases where the initial assessment is not sufficiently precise and there is need of a more detailed investigation of the structural behaviour and load-carrying capacity, the enhanced level of structural analysis can be used (see multi-level assessment strategy in Figure 2). However, enhanced structural analysis is rarely used in bridge assessment and, therefore, a common engineering practice has not been developed. In order to support analysts with the large number of modelling choices, this section presents a framework for nonlinear FE modelling with application to the specific bridge studied in this paper. Thus, the failure test of the Kiruna Bridge was also used to evaluate the multi-level strategy at the enhanced level of structural analysis in conjunction with the nonlinear FE modelling framework. Since the initial assessment of the bridge indicated the importance of modelling the capacity with regard to shear more precisely (see Section 6.2), the enhanced assessment was carried out at Level 3 of the multi-level strategy. This means that both flexural and shear-related failures are implicitly simulated in the structural analysis.

In assessments, it is of importance to take into account the actual structural conditions and the impact of eventual deterioration. However, for this particular case study, it was possible to consider the bridge as intact due to its good condition (see Section 3.1).

5.1 Nonlinear FE modelling framework

A framework for nonlinear FE analysis is summarised below and applied in assessment of the Kiruna Bridge. It is based on the guidelines by Hendriks et al. (2017) and adapted for use with ATENA Studio (ATENA 2016b). The general guidelines, provided by Hendriks et al. (2017) with previous editions by Hendriks et al. (2012) and Hendriks et al. (2016), compromises both RC and PC beams and slabs under static loading (similar to the scope of the multi-level strategy). In the presented modelling framework, the recommendations in the general guidelines were primary used over and above others, and where these recommendations were insufficient, modelling choices (sometimes undocumented) provided by ATENA (2016b) were used. In particular, it was necessary to deviate from the guideline regarding the type of concrete constitutive model recommended (the total or composed strain concepts) in order to use the

ATENA software. Furthermore, in some specific cases, the recommendations were not strictly followed due to practical issues, particularly associated with reduction of the computational effort needed (see descriptions and discussions in subsequent sections).

The first step in the modelling of the structure is to idealise it to a mechanical model and secondly to discretise it to a FE computational model. These steps should be carried out carefully because of their great importance to the response in the analysis. Depending on the problem investigated using FE analysis, either the whole structure, single components or only critical regions can be included in the model. It is often effective with respect to the modelling and computational effort to model different structural parts with different degrees of detailing, to obtain representative boundary conditions for the region of particular interest without having the whole structure in detail (Broo et al. 2009). Due to the large scale of the structure and the need to minimise the computation effort, varying detailing was used for different parts of the Kiruna Bridge. In the failure critical regions (blue in Figure 6) a finer mesh with continuum elements was assigned to the structure, but outside these regions, the same same discretisation as in the initial assessment was used. Furthermore, in regions reaching cracking or nonlinear compressive response, a nonlinear constitutive model was used for the concrete while a linear elastic material model was used outside this region.

The current condition of the structure is of particular importance when assessing existing bridges, although it is only sparingly accounted for in the abovementioned guidelines. It has to be considered in the nonlinear FE model of the structure in order to accurately assess the structural behaviour and load-carrying capacity and, thus, inspection of the actual structure is essential (see bridge assessment approach in Figure 1). In Hendriks et al. (2017), some recommendations are provided for how existing cracks, caused by previous loading events, can be taken into account. Existing cracks can be treated by either: (1) locally reducing the modulus of elasticity, tensile strength and fracture energy or (2) simulating the crack formation with additional load cases. However, the guidelines do not specify the magnitude of reduction to use for (1), which may be crucial in reflecting the current structural behaviour. Other mechanisms leading to deterioration of the structure are, for instance, reinforcement corrosion, freeze-thaw cycles and

alkali-silica reactions. These can usually be taken into account by altering the geometry, using up-to-date material properties of concrete and reinforcement materials, and using current knowledge of their interactions (Hanjari et al. 2011, 2013). However, in the enhanced structural assessment of the Kiruna Bridge, it was possible to ignore the presence of deterioration that had occurred prior to the experimental investigation due to the current good bridge condition (i.e. the bridge was considered to be intact).

5.2 Boundary conditions and loads

5.2.1 Boundary conditions

In order to simulate the structural behaviour, the boundary conditions should be properly defined. Apart from the boundary conditions for supports, the connections between structural parts need to be modelled, for instance, joints and interfaces between different types of elements. Another issue of importance for analysis of bridges is the soil-structure interaction, which may have an influence on the structural behaviour (Dutta & Roy 2002). This interaction can be included by discretely modelling the foundation system together with the surrounding material. Alternatively, springs simulating the deformation properties of the foundation soil/bedrock can be used to simplify the model.

In the Kiruna Bridge model, the boundary conditions applied were identical to the initial structural assessment (see Section 4.1), except for the joints between the columns and the foundation at the intermediate supports. In the tests, the vertical concrete strain was measured 800 mm from the bottom of the columns in the centre line of each column side (Bagge et al. 2014). The externally applied loads were consistent with the forces derived from the measured strains. However, the strains measured also showed flexural moment in the columns, indicating rotational restraints in the joints between the column and the foundations, not included in the initial structural assessment. Based on these observations, a rotational restraint stiffness was derived and applied using rotational springs connected to the bottom surface of the columns.

5.2.2 Loads

All relevant loads affecting the structure have to be taken into account in the nonlinear analysis and the critical load combination is preferably determined beforehand using simplified analysis. Dead weights of the structure and other permanent loads should be applied in initial load step(s). Thereafter, the most unfavourable combination of variable loads should be incrementally applied in subsequent load case(s) (Hendriks et al. 2017), with sufficiently small increments to account for local and global effects. In this way, the nonlinear response can be obtained.

For analysis of the ultimate load-carrying capacity of RC structures, it can be beneficial to load the structure using displacement control, in which the external loads are controlled by successively increased point displacement. Such deformation-controlled loading, particularly useful for concentrated loads, usually yields a more stable numerical analysis in comparison to force-controlled loading. Hendriks et al. (2017) stated that displacement-controlled loading is not suitable for multiple loads; however, a procedure to model combinations of loads was described by Broo et al. (2009) and applied to traffic loads composed of multiple concentrated loads.

In the first step of the simulation of the experimental test, dead weights and prestressing were assigned to the structure in a single load increment. In the test, the pavement was removed from the structure and, thus, only the concrete was taken into account with a load intensity of 24 kN/m^3. The residual prestress force was introduced in accordance to the evaluation described for the initial structural assessment. In the second step of the analysis, the dead weights of the loading equipment were included in one load increment with a load intensity of 78.5 kN/m^3, yielding a total load of 170 kN.

To simulate the external loading, the same loading procedure was used as for the test. The load distribution beams and load distribution plates in contact with the top of bridge deck slab were included in the FE model in order to simulate the distribution of forces accurately and to avoid numerical problems possibly occurring when applying concentrated forces at single points (see Figure 6). The simulation involved the following steps:

1. Symmetric force-controlled loading up to a total of 6 MN, followed by unloading to represent the actual preloading procedure (10 + 10 load increments) used.
2. Symmetric force-controlled loading up to 12 MN (20 load increment).
3. Displacement-controlled loading with increments of 20 mm in the location of the outer jack adjacent to the south girder (corresponding to Jack 1 in Figure 3). This loading continued until structural failure occurred.

5.3 Constitutive models

5.3.1 Concrete

For the nonlinear modelling of concrete, a range of constitutive models exists; here, only the one used is described among many found in the literature. The constitutive model for concrete in 3D implemented in ATENA Studio is called *CC3DNonLinCementitious*, see Figure 7 (Červenka & Papanikolaou 2008). The model combines the fracture mechanics of concrete in tension, following the smeared crack concept with the Rankine failure criterion, with plasticity theory of concrete in compression, with a Menétrey-Willam failure surface for the triaxial stress state (Menetrey & Willam 1995). In contrast to the recommendation from Hendriks et al. (2017) to use the total strain concept, the implemented model is based on the strain decomposition concept (de Borst 1986) separating the elastic, plastic and fracturing strains in order to ensure compatibility between the fracture and plasticity models.

In order to model the concrete behaviour accurately, material characteristics derived from the structure of interest should be used. However, in the absence of information from *in situ* tests, the modulus of elasticity E_c, the tensile strength f_t and the fracture energy G_f can be approximately determined from the concrete compressive strength f_c. In the nonlinear FE model, mean values should be used in order to predict as realistic a behaviour of the structure as possible.

In the predefined stress-strain relationship in *CC3DNonLinCementitious,* the concrete is assumed to behave linearly until tensile strength f_t is reached, or until a stress level corresponding to $2f_t$ is reached in

compression. After crack initiation, an exponential softening is used for the normal stress in the crack, σ, based on (Hordijk 1991), see Equation (1) and Figure 7(a):

$$\sigma = f_t \left\{ \left[1 + \left(c_1 \frac{w}{w_c} \right)^3 \right] \exp\left(-c_2 \frac{w}{w_c} \right) - \frac{w}{w_c} \left(1 + c_1^3 \right) \exp\left(-c_2 \right) \right\} \quad (1)$$

where f_t is the tensile strength, w is the crack opening, w_c is the crack opening at complete release of stress and c_1 = 3 and c_2 = 6.93, being constants for normal weight concrete. In order to transform the crack opening to strain, a crack band model is introduced. The crack band size, L_t, represents the width over which a crack localises in a smeared crack analysis, and the crack strains are determined by dividing the crack opening with the crack band width. The original purpose of using the crack band approach was to reduce the influence of element size and orientation (Bažant & Oh 1983; Rots 1988). According to Červenka et al. (1995), satisfactory results could be obtained by assuming a crack band size equal to the size of the element in the direction perpendicular to the cracks (see the finite element in Figure 7(a)).

However, in cases of heavily reinforced concrete structures or large finite elements, cracking can not localise into separate brack bands in the analysis and such assumption will give a too brittle response. In these cases it is more reasonable to divide the crack opening with an estimated crack distance to obtain the crack strain, see Plos (1995). It is recommended that the user manually specifies a crack spacing in such cases; this can subsequently be used as the crack band size. Hendriks et al. (2017) proposed to estimate the maximum crack spacing $s_{r,max}$, in accordance with the European standard (SS-EN 1992-1-1 2005)

The concrete response in compression was defined by ATENA (2016b) as a strain-based parabolic ascending branch describing the hardening and a displacement-based linear descending branch describing the softening (see Figure 7(b-c)). Equation (2) is the parabolic expression for the normal stress:

$$\sigma = f_{c0} + \left(f_c - f_{c0} \right) \sqrt{1 - \left(\frac{\varepsilon_c - \varepsilon_{eq}^p}{\varepsilon_c} \right)^2} \quad (2)$$

where f_{c0} is the stress at onset of nonlinear behaviour, f_c is the compressive cylinder strength, ε_c is the strain and ε_{eq}^{p} is the plastic strain at compressive strength. Generally, the maximal displacement w_d in the linear softening is suggested as being 0.5 mm (van Mier 1986). In order to reduce the mesh size dependency, the transformation of strains to displacements is carried out using a length scale parameter L_c given for the element size in the direction of principal compressive stresses, analogous to the crack band size L_t. (see finite element in Figure 7(c)). In the guidelines provided by Hendriks et al. (2017), multi-axial compression interaction needs not to be included, leading to a conservative assumption. However, the material model used provides a triaxial failure surface, based on the theory of plasticity, to take the positive confinement effect into account (Červenka & Papanikolaou 2008).

If the concrete is simultaneously loaded in tension and compression in different directions, the compressive strength is reduced due to cracking; the guidelines by Hendriks et al. (2017) required this interaction to be included. For the material model used, a proposal by Vecchio and Collins (1986) is introduced, one that implies the strength is reduced to $r_c f_c$. The compressive strength reduction r_c is given by:

$$r_c = \frac{1}{0.8+170\varepsilon_1} \quad \text{and} \quad r_c^{\lim} \le r_c \le 1.0 \tag{3}$$

where ε_1 is the maximal principal tensile strain of the cracked concrete and r_c^{lim} is a limitation of the strength reduction. Studies of the strength reduction factor show a variation in the limiting value: 0.45 according to Kollegger and Mehlhorn (1988), 0.80 according to Dyngeland (1989) and ATENA (2016b), and 0.40 according to Hendriks et al. (2017).

There are two types of smeared crack concepts, either fixed or rotating crack models, recommended in Hendriks et al. (2017), both implemented in *CC3DNonLinCementitious*. The material model also provides a combination of the concepts, implying that the rotating crack concept is used to a certain level where the crack direction is fixed. In ATENA (2016b), it is suggested that the shift occurs at a residual tensile strength between 60 % and 90 % of the initial tensile strength, according to the experience from the developer of the material model. Assuming a fixed direction of the cracks, resulting in stress-locking

phenomena, may lead to overestimation of the failure load (Rots 1988) and, therefore, a shear retention model reducing the shear stiffness should be used in nonlinear FE analysis of concrete structures (Hendriks et al. 2017).

Due to a variation in the shear stiffness at the crack opening, ATENA (2016b) proposed that the shear stiffness of the crack should be linearly coupled to stiffness perpendicular to the crack using a shear stiffness reduction factor s_F. Based on experimental work by Walraven (1981), the recommended value of the shear stiffness reduction factor is 20. However, this value is considered conservative for some cases and the developer of the material model has (undocumented) used values as high as 200 to give more accurate results. In the material model *CC3DNonLinCementitious,* the favourable influence of the aggregate interlock on the shear strength of a crack is also taken into account. Here, equations from the modified compression field theory (MCFT) by Vecchio and Collins (1986), based on observations by Walraven (1981), have been used.

According to the guidelines by Hendriks et al. (2017), the tension stiffening effect due to the interaction between the concrete and reinforcement is essential for the load-carrying mechanism and should be taken into account, although no recommendation of how to do this is provided. If the bond-slip relationship between the reinforcement and the concrete is not implicitly included in the FE model, the tension stiffening effect can be approximated by modifying the tension softening relationship of the concrete in tension. In *CC3DNonLinCementitious,* the tension stiffening is taken into account by limiting the tensile stress to a certain value in the relationship for tension softening.

Thus, the stresses are prevented from dropping below the level specified. The default value in the software is 40 % of the tensile strength with reference to Model Code 1990 (CEB-FIP 1993), but (undocumented) experience from the developer of ATENA (2016b) indicates that this level is high and can lead to overestimations of the structural stiffness and the load-carrying capacity. Instead, typically 10 % to 20 % of the tensile strength is recommended for relatively dense reinforced regions and the default level can be considered as a maximum in extreme regions. Moreover, levels in the range between 1 to 5 % of the tensile strength can be useful in sparsely reinforced regions to stabilise the analysis.

In the analysis of the Kiruna Bridge, due to the computational effort required, only the parts of the bridge where cracks were expected to form were analysed using the nonlinear concrete constitutive model (*CC3DNonLinCementitious*); the rest were modelled using linear elastic material response. For the modulus of elasticity (E_c = 32.1 GPa) and the concrete compressive strength (f_c = 62.2 MPa), tested mean values were used (see Section 3.3). In the absence of tested tensile properties of the Kiruna Bridge, the tensile strength (f_t = 2.0 MPa) and fracture energy (G_f = 140 N/m) were estimated based on a prior study (Puurula et al. 2015). In the earlier study, *in situ* experiments on a 51 year-old RC bridge, constructed at the same time and using a similar type of concrete, were carried out. From these, a tensile strength of 2.2 MPa and fracture energy of 154 N/m were obtained for a concrete with compressive strength of 68.5 MPa. In addition, studies of compiled *in situ* material tests for existing concrete bridges by Thun et al. (1999, 2006) showed a considerably improved concrete compressive strength, compared to values from the design of the bridge, while the tensile strength did not increase to the same degree. Thus, the relationships stated in the Model Codes 1990 and 2010 (CEB-FIP 1993; fib 2013), and suggested in the guidelines by Hendriks et al. (2012) and Hendriks et al. (2017), between the compressive strength and tensile strength and fracture energy, respectively, are probably not representative and so not to be recommended generally for the assessment of existing bridges.

Untested characteristics, such as the Poisson's ratio (ν = 0.15), the limiting compressive strength reduction factor (r_c^{lim} = 0.40) and the crack spacing (L_t = 200 mm), were determined using the guidelines by Hendriks et al. (2017). Regarding the level for the shift from rotating to fixed crack model (c_{fc} = 0.6), tension stiffening (c_{ts} = 0.01) and the shear stiffness reduction factor (s_F = 20), no instructions are provided in the general guidelines and, consequently, (undocumented) recommendations from the developer of the ATENA software were strictly followed, based on assumptions expected to be conservative. The impact of aggregate interlock was taken into account with the MCFT by using a maximal aggregate size (a_g = 32 mm). Parameters directly related to the shape of the stress-strain curve in compression and the failure surface were determined from suggestions from ATENA (2016b).

The extent of the region behaving nonlinearly was determined through a successive extension of the nonlinear part until no strain exceeding the level of initiated concrete cracking was observed outside this region. Based on this procedure, approximately $^1/_2$ to $^2/_3$ of the spans adjacent to the externally loaded span were modelled with a nonlinear material model, see Figure 6(a). The remaining part of the bridge, consisting of foundations, columns, girders, cross-beams and deck slab, was modelled using elastic material properties (E_c = 32.1 GPa, ν = 0.15). Elastic material properties were also assigned to the bearings and load distribution beams and plates (E_s = 210 GPa, ν = 0.30).

5.3.2 Reinforcement

The constitutive response for the reinforcement needs to be adapted to the specific reinforcement material. The material properties can either be assumed using values from the codes, or determined based on *in situ* tests on samples from the structure. In the model, mean values should be used. For non-prestressed and prestressed reinforcing steel, the post-yield hardening should be included in the model, not only due to its significant contribution to the load-carrying capacity, but also for its stabilising effect on the analysis. A simplified elasto-plastic constitutive model with hardening, represented by the elastic modulus, yield strength, tensile strength and strain at the maximal force, is acceptable according to the guidelines by Hendriks et al. (2017). Reinforcement consisting of fibre-reinforced polymers does not have any post-yield hardening, and the constitutive model is only represented by an elastic response until the ultimate strain is reached. Although a simplified stress-strain relationship is acceptable according to the guidelines, the ATENA Studio enables a more precise user-defined relationship to be used that allows, for instance, the response of the rupture to be included.

In the analysis of the Kiruna Bridge, the post-yield hardening was included with a multi-linear stress-strain relationship based on tensile tests in the constitutive models used for all the reinforcing steel (see Figure 8). Thus, a more accurate simulation of the yielding, hardening and, ultimately, the strain softening was achieved compared to one based on the recommendations in Hendriks et al. (2017). Moreover, the strengthening using NSM CFRP in the soffit of the central girder was modelled with a

linear stress-strain behaviour until rupture occurred at the ultimate strain limit. As for the initial structural assessment, the prestressed CFRP laminates were excluded from the FE model due to premature debonding.

5.3.3 Material interaction

In addition to the constitutive model for the individual materials, it is necessary to make assumptions about their interaction. The main mechanisms associated with concrete reinforcement interaction are bond-slip behaviour, which can cause splitting stresses and possibly anchorage failure, the tension stiffening effect and dowel action. Without making further recommendations, the guidelines by Hendriks et al. (2017) state that modelling bond-slip behaviour for the interaction between the reinforcement and surrounding concrete enables more accurate predictions by the nonlinear FE analysis. A perfect bond is suggested as being a sufficiently good approximation in most cases, but in calculation of crack widths and in investigations of member ends and anchorage regions, a bond-slip relationship is preferable. The models of bond behaviour available in ATENA (2016b) include, in addition to assuming a perfect bond, a bond-slip relationship developed by Bigaj (1999), one recommended by Model Code 1990 (CEB-FIP 1993) or a user-defined relationship.

According to ATENA (2016b), if the bond-slip response is not included in the FE analysis, the tension stiffening effect can be included as a part of the concrete constitutive model, as previously described. However, in none of the guidelines is a model for including the dowel effect recommended or implemented, although it can be accounted for through the choice of finite element type for the reinforcement. Due to the type of problem, without focus on crack widths and anchorage regions, the reinforcement was assumed perfectly bonded to the concrete in the FE model of the Kiruna Bridge. This followed the suggestion by Hendriks et al. (2017).

5.4 Finite element modelling

When modelling using FEM, the mechanical model representing the structure is divided into finite elements. In this step of the modelling, aspects such as element types, interpolation degree and numerical

integration scheme are chosen to ensure a simulation that reproduces the behaviour of interest. The 3D continuum elements can be considered as the most suitable for detailed modelling, handling flexural as well as shear type failures. Shell elements model flexure as well as in-plane shear failures, while beam elements, in general, only model flexural failures with high precision. Due to the computational effort required, continuum elements cannot always be used for entire large-scale structures. Consequently, the discretisation of the structure should be carried out carefully, using different elements depending on the structural part, the loading and the possible types of failure modes.

For the modelling of concrete and reinforcement, Hendriks et al. (2017) generally recommended quadratic interpolation of the displacement field within continuum elements in order to simulate the deformation modes better. However, the developer of ATENA advocated the use of linear interpolation with half mesh size, referring to that the nature of the cracking of concrete leads to discontinuities in terms of displacements and stresses, which violate the assumption of smoothness in quadratic elements. Where structural elements (truss, beam and shell elements) are used, which may help reduce the computational effort required, 3-node beam elements and/or 6-node or 8-node shell elements are preferable.

In ATENA (2016b), the reinforcement is preferably modelled as embedded bars in the concrete, with the option of discrete reinforcement bars or smeared layers in the beam, shell or continuum elements. Most commonly, discrete reinforcement bars are modelled with truss elements. These 1-D truss elements only have axial stiffness and to include dowel effects, either beam or continuum elements would be needed for the reinforcement. It is recommended that the elements representing the concrete follow a full integration scheme in order to avoid spurious modes, while a full or reduced scheme is acceptable for the reinforcement due to embedded elements inhibiting spurious modes. In ATENA (2016b), the available elements, with a few exceptions, follow the Gaussian integration scheme fulfilling the requirement for full integration.

Since the nonlinear FE analysis is sensitive to the quality of the finite elements, a meshing algorithm, minimising the element distortion, should be used. Parameters that should be minimised are

the aspect ratio, skewness and area to perimeter ratio (Hendriks et al. 2017). The guidelines do not propose a minimum size of element since this is governed by its influence on the computational effort. The maximal element size is stated as being more crucial in avoiding a snap-back response in the constitutive models and for obtaining smooth, continuous stress fields, which may be hard to achieve with too large elements (Hendriks et al. 2017). In order to avoid the snap-back response, the maximal size of continuum elements is recommended to be limited so that the elastic energy in the elements at crack initiation is less than half of the fracture energy, which can be estimated using:

$$L_t < \frac{E_c G_f}{f_t^2} \tag{4}$$

where E_c is the modulus of elasticity, G_f is the fracture energy and f_t is the tensile strength.

In addition, Hendriks et al. (2017) proposed the maximal element size to be less than that given in Table 3. A recommendation from the developer of ATENA Studio is to use four to six continuum elements to model the whole height in order to capture the flexural behaviour of the structural part. The same number of layers and cells are recommended for quadratic shell and beam elements, respectively. Moreover, an aspect ratio of the finite elements not larger than three to four is recommended, in order to provide a good mesh quality. However, such requirements, ensuring the quality, are lacking in the general guidelines by Hendriks et al. (2017).

This bridge was modelled with different degrees of detailing in the finite element idealisation and discretisation, depending on the expected behaviour of different structural parts, see Figure 6. In addition to the type of elements, with their capability to simulate different behaviour, the quality of the mesh and the computational effort required were taken into account. In Table 4, the usage of the volumetric elements are summarised with approximate maximum element size in the global directions of the bridge. For all the elements, the quadratic interpolation was used as recommended by Hendriks et al. (2017). For the beam and shell elements, the internal cross-sectional composition of elements was specified in terms of number of cells and layers, respectively. In the longitudinal direction(s) of the elements, two integration points for beam elements and three integration points for shell elements were used.

Further explanation of the concept can be found in ATENA (2016b). For the parts of the bridge simulated as exhibiting a linear behaviour, beam elements (*CCIsoBeamBrick*) represented columns, girders, curbs and cross-beams while shell elements (*CCIsoShellBrick*) represented foundations, deck slab and loading plates, and the components of the load distribution beams. In order to take the shear response into account in the girders and cross-beams in the nonlinear region, the beam elements were replaced by continuum elements (*CCIsoBrick*). By having only one element across the width of the beams, their transversal shear behaviour could not be reflected. Moreover, continuum elements were used for the slab locally at the point of application of the external loads to the bridge, where the out-of-plane shear could be expected to be of importance (see Figure 6), but were avoided elsewhere to reduce the computational effort required.

Due to the size of the FE model and limited computational resources, it was preferable to vary the element sizes based on their importance for the structural behaviour. Thus, the finest mesh was assigned to the region adjacent to the external loading where the final failure was expected, with gradually coarser mesh used for the remaining nonlinear and linear parts of the bridge (see Figure 6). In the nonlinear part, the general recommendations specified in Table 3 were followed, combined with the minimal element size of 560 mm given by Equation (4). In order to ensure there was no significant influence of mesh size on the outcomes of the simulation, a mesh sensitivity study was carried out. The element sizes in the nonlinear region were halved in each direction, following the procedure for the mesh sensitivity study according to the recommendations in Broo et al. (2008).

The prestressed steel reinforcement tendons and NSM CFRP rods were modelled as discrete truss elements (*CCIsoTruss*). The non-prestressed reinforcement was generally modelled as smeared (or embedded) reinforcement in the concrete elements. However, in the region of highly stressed concrete, the longitudinal non-prestressed reinforcement was modelled with discrete truss elements in the girders and the cross-beams. Discrete truss elements were also used to represent both the longitudinal and transverse reinforcement in the slab, locally close to the external loading, as well as for the stirrups in the

girders (for the entire span except for 4.0 m adjacent to the supports). The truss element sizes were consistent with the surrounding concrete elements.

5.5 Solution methods

In order to take the nonlinearities of the structure into account, an iterative procedure is required to find the equilibrium of internal and external forces. The most common methods used to find the equilibrium are based on the Newton-Raphson method (Ypma 1995); when potential snap-back behaviours are to be taken into consideration, arc-length methods are popular (Riks 1970; Wempner 1971). In the modified Newton-Raphson method, the stiffness is calculated in the first iteration of each load increment only, instead of at each iteration. Thus, the computational time can be reduced in the case of time-consuming stiffness calculations, although additional iterations are usually required. In these methods, a certain degree of imbalance can be allowed between internal and external forces, and the convergence criteria are recommended to be defined as the error in terms of displacement (1 %), residual force (1 %) and energy (0.01 %) with the values proposed by Hendriks et al. (2017) specified in brackets. The same values are recommended by ATENA (2016b). However, the tolerances stated are not proven and, in most cases, errors of about 2 % in terms of displacement or residual force in a single step do not cause a problem, but errors above 10 % in several steps mean that the result should not be regarded as reliable (ATENA 2016a). Simulations of the loading of RC structures often fail to reach convergence when cracking is initiated and close to the ultimate load limit, so it can be beneficial sometimes to proceed with the analysis although the convergence criteria have not been fulfilled. If this happens, the reliability of the results from the simulation should be evaluated based on the convergence criteria (Broo et al. 2008).

Modified Newton-Raphson solution methods were applied in the FE simulation of the bridge failure test in order to minimise the computational effort. The recommended convergence criteria were used and, in the case where the specified upper limit of iterations (500) was reached, the solution from the iterations with the lowest error was used for further analysis.

6 Results and discussion

6.1 Description of the experiment

At a total externally applied load of 13.4 MN, the south bridge girder and its connected slab suddenly failed after relatively large deformation (about 180 mm) and extensive cracking in the midspan region. The load was distributed, as shown in Figure 4, with 5.4 MN in the outer hydraulic jack adjacent to the south, first-to-fail girder (Jack 1), 2.0 MN in each inner jack adjacent to the central girder (Jacks 2 and 3) and 4 MN in the outer jack adjacent to the north girder (Jack 4). Here, the failure occurred at the peak load, with a subsequent load drop. Due to the testing procedure, with the equally-distributed loading changed at 12 MN in order to fail the girders one at the time, the load-carrying capacity of the whole superstructure can be expected to be even higher than 13.4 MN for the situation where there is a more equal distribution of the loads.

The experimental failure is shown in Figure 9 with the measured load-deflection response of the three bridge girder at their midspan shown in Figure 10(a). Shortly after the peak load, the sensors measuring the deflection were disturbed, particularly on the south girder, and, thus, the descending load-deflection curve is not included in the graphs. During the loading, a highly nonlinear response of the bridge superstructure took place. However, in Figure 10(a) the reduced stiffness associated with crack initiation is not captured, since the girders were cracked during the preloading schedule and the stiffness was therefore already reduced at the start of the failure loading.

Video monitoring of the failure mechanism indicated that the failure started in the slab and the upper part of the girder due to diagonal tension cracking, followed by rupture of the stirrups crossing the crack (see Figure 9(c)), first on the west side of the load (left in Figure 9(a)) and then on the east side of the load. The loading plate on the bridge deck slab was punched through the slab, meaning out-of-plane shear in the slab (Figure 9(d)), at the same time as a shear failure took place in the girder (Figure 9(c)). The diagonal crack east of the midspan was located across the region of the prestressing system anchorage devices. In the anchorage region, the concrete section widened from 410 mm to 550 mm. As

expected, this increased the stiffness and shear resistance of the girder locally and, thus, the localisation of the failure. Moreover, the capacity of the slab was slightly reduced due to the holes drilled through it to provide space for the cables between the bedrock and the hydraulic jacks. One hole was drilled 885 mm from the centre line of the girder and likely influenced the ultimate load-carrying capacity as a consequence of the failure surface of the slab intersecting the hole.

At a relatively modest load of about 9.0 MN, the prestressed CFRP laminates on the south girder prematurely debonded. This was caused by inadequate bonding after the installation, since the base of the girder was not completely flat (i.e., concave) as required by a strengthening technique that used prestressing. Due to the small concaveness, not discernible before strengthening, the laminates were straightened, pulled and finally debonded from the concrete surface. However, this change of the structural system did not have any notable impact on the overall behaviour of the bridge (see measured response in Figure 10(a)). In contrast, the NSM CFRP rods on the central girder worked as intended up to the failure load, and based on these findings, only the strengthening of the central girder was taken into account in the analysis of the experimental test.

Subsequent to the failure at the south girder, the load dropped to 11.4 MN (see Figure 4) before the central girder was further investigated by increasing loads with the inner hydraulic jacks (Jacks 2 and 3). A similar failure mechanism took place in the central bridge girder, as for the south girder, at a total load of 12.8 MN. This indicates a remarkable robustness of the structure, with an essential residual load-carrying capacity, despite that the south girder failed (but not collapsed). However, this second part of the test is not further described in this paper.

In order to monitor the behaviour of the bridge during the test, measurements were carried out according to the programme summarised in Section 3.4. The strains were locally measured on stirrups using strain gauges attached in positions indicated in Figure 9(c). During the preloading of the bridge, a diagonal crack formed across the position of sensor SG 4 and yielding was consequently measured for a load lower than 6.0 MN. This finding explained the initially high strains also measured in the failure test (see Figure 10(b)). At the same time as the formation of the crack crossing sensor SG4, the final critical

crack was formed. Nonetheless, the sensors adjacent to the critical crack indicated relatively modest strains, as a consequence of the crack not crossing the exact positions of the gauges. After further crack formation, yielding of the stirrup was detected where sensor SG8 was located, at a load of 12 MN, and where sensor SG7 was located at the failure load, see load-strain relationships in Figure 10(b). During the latter part of the loading sequence, high strains were also indicated by SG5 due to a crack crossing the measured position of the stirrup.

6.2 Initial structural assessment

Analysis of the bridge test at the initial levels of the multi-level structural assessment strategy (Level 1A – 1B) resulted in the load-carrying capacities in Figure 11. The load-carrying capacity, expressed as externally applied load, is shown both with respect to the moment and the shear resistance according to the procedure described in Section 4. The capacities are determined with material properties as specified in the assessment code or as *in situ* material properties, respectively.

Improving the accuracy of the material properties generally gave an appreciably higher shear capacity, mostly due to the 21 % higher yield strength of the stirrups (see Table 2). However, the moment capacity was almost unaffected, indicating that the concrete strength only had a small influence even though it had increased by 75 % (see Table 1). This small increase in moment capacity can be explained by the prestressed reinforcement, with only a marginally increased tensile strength, being governing for the resistance.

Comparison of the theoretically determined shear resistances with the shear caused by the action effects according to the linear elastic analysis clearly indicates, independent of the level of approximation in the Model Code 2010 (fib 2013) (denoted MC I – III), that the shear resistance is critical rather than the moment resistance. In contrast, the European standard (SS-EN 1992-1-1 2005) (denoted EC2), gives marginally lower shear capacity in comparison to the moment resistance using the material properties from the assessment code, the shear resistance governs the load-carrying capacity only after plastic moment redistribution (i.e., structural analysis at Level 1B of the multi-level assessment strategy).

The main reason for the difference between the shear resistance according to the Level I approximation in the Model Code (MC I) and the European standard (EC2), both relying on a variable-angle truss model approach, is the lower limit of the angle of compression strut inclination (18.4º in EC2 compared to 25º in MC I). Here, it should also be noted that the location of the shear failure predicted by these two models was adjacent to support 2, which does not agree with the experimental findings. The high flexural moment at the midspan is one cause of the inconsistency between the experimental test and analysis, since the interaction between flexure and shear is ignored in the resistance models.

Moreover, previous studies of the variable-angle truss model, applied to girders, also show a large scatter in prestressed concrete members, members with a T-shaped cross-section and members with low reinforcement ratios (e.g., see Cladera and Marí 2007). In the local resistance models at the Levels II and III approximations in the Model Code, the flexure and shear interaction is accounted for through the mid-depth strain given by the actual action effects. As in the test, the shear failure was predicted to occur on either side of the external loading at the midspan. However, the higher level models predicted a considerably lower load-carrying capacity but, in terms of the angle of compressive field inclination, the results were consistent. According to analysis at Levels II and III using *in situ* material properties, the inclination was 49° and 50°, respectively, whereas approximately 50° – 52° was observed in the test of the south girder (see Figure 9(a-c)).

The differences between the experimental and the theoretical outcome from the higher level models are related to several factors. A part of the difference can be associated with: (1) the full tensile strength of the stirrups including the post-yield hardening not being taken into account in the resistance model, (2) the contribution of the flange of a T-shaped girder (i.e., the bridge deck slab) being ignored in the resistance model, and (3) the distribution of action effects in the test differing from the response given by the structural analysis.

As stated above, the distribution of action effects can be regarded as one uncertainty in the initial assessment of the load-carrying capacity. In order to reduce the uncertainties it would therefore be preferable to improve the structural analysis by using nonlinear simulations at enhanced levels (i.e.,

Levels 2 – 4) in the multi-level structural assessment strategy. In order to accomplish a further improvement of the structural analysis and to investigate the shear behaviour more precisely, analysis at Level 3 is necessary. This analysis does not rely on a specific local resistance model, which, in some cases, has been shown to predict failure at the wrong location and in others given a very conservative load-carrying capacity.

6.3 Enhanced structural assessment

Enhanced assessment of the structural behaviour and load-carrying capacity was carried out at Level 3 of the multi-level structural assessment strategy following the nonlinear FE modelling framework described in Section 5, with use of *in situ* measured boundary conditions at the base of the columns and with tensile properties based on prior experience regarding the actual concrete. Furthermore, the quality of the mesh and, thus, the validity of the model, were also checked in accordance with the previously described mesh sensitivity study.

Figures 12(a-c) present a comparison between the simulated bridge behaviour and the experiment in terms of the load-deflection response of each girder. From these curves, the consistency between the theoretical and experimental behaviour can be seen. The nonlinear FE analysis yielded a load-carrying capacity of 13.9 MN that was very precise in relation to the test (overestimate by 3.8 %). However, the FE model indicates a more ductile structural response, with larger deformations of the girder at the peak load and without a sudden load drop thereafter. This can partly be explained by differences in the loading procedures; in the analysis, displacement-controlled loading was used above 12.0 MN for stabilisation of the FE analysis, while force-controlled loading was used in the experimental test, leading to a more dramatic failure mechanism with a different post-peak behaviour. The load-deflection curves also shows a small mesh size dependency for the mesh size specified in the nonlinear FE modelling framework. Using finite elements with half the recommended dimensions yielded a load-carrying capacity of 13.6 MN (overestimate of 1.4 %), a somewhat smoother load-deflection response, and improved stability of the analysis in terms of convergence. A drawback of the reduced mesh size was the appreciable increase in

computational effort, and consequently the analysis only included the initial part of the descending branch.

In order to evaluate the failure mechanism in the bridge test simulation, the reinforcing steel strains were measured in the tendons and stirrups. These measurements are presented in the load-strain curves in Figure 12(d), extracted from the position of highest strain at the peak load with external loading concentrated on the south girder. At a load level of about 11 MN, the 0.2 % proof strength was reached for the prestressing steel. Shortly thereafter, yielding was initiated in the stirrups with a stain of 6 % at the peak load, and in the final part of the subsequent descending branch (excluded in Figure 12(d)) the ultimate steel strain was reached. Thus, a shear-related failure with rupture of the stirrups was indicated as observed in the experimental test. Moreover, the simulation and experimental test resulted in similar strain evolutions (compare Figure 12(d) and Figure 10(b)), although the *in situ* measurements were performed in predefined, fixed positions with a limited measuring range of the strain gauges. The load-strain curves in Figure 12(d) also indicated an acceptably small mesh size dependency.

The nonlinear FE analysis predicted formation of both vertical flexural cracks and inclined shear cracks in the midspan region, adjacent to the externally applied load. The major principal concrete strains and elements with crack widths larger than 2 mm are shown in Figure 13 for the ultimate load. Similar to the experimental test (see Figure 9), the simulation indicated failure initiation in the slab with extensive cracking along, and parallel to, the girder on either side of it, and simultaneous diagonal cracking in the girder and through the slab. The comparison of Figure 9(a) and Figure 9(b) also shows consistency when reducing the size of the finite elements in relation to the recommendations. However, with the finer mesh, a more distinctive inclined shear crack was obtained.

It can be concluded that the enhanced structural analysis at Level 3 of the multi-level assessment strategy, following the framework for nonlinear FE modelling, resulted in a precise analysis of the complex bridge failure. The predicted load-carrying capacity was close to the experimental value and the failure mechanism, governed by out-of-plane shear failure of the slab and a combined flexural-shear failure of the girder, was reproduced. However, during the bridge modelling and the associated

simulations of the test, several important modelling aspects were identified. It was crucial to model the bridge slab around the application of the external loading with continuum finite elements and sufficiently fine mesh to reflect the out-of-plane shear response in the slab. Moreover, using representative boundary conditions and concrete tensile properties were required in order to obtain precise and reliable results.

6.4 Sensitivity study

Within the framework for nonlinear FE analysis, large numbers of modelling choices are involved. In the framework, described by Hendriks et al. (2017) and ATENA (2016b), the recommendations are based on common practice and prior experiences (sometimes undocumented). There are also cases of contradictions in the different guidelines. Thus, it still remains for the analyst to make appropriate assumptions in the modelling of the specific structure and associated loading. An extensive sensitivity study was carried out in order to map some of the most influential parameters, highlight aspects in need of further investigation and consideration in the guidelines and, ultimately, to support better understanding and facilitate improved FE analyses of existing structures.

The sensitivity study examined the modelling parameters' impact on the simulated structural behaviour of the bridge, utilising the previously described FE model for enhanced analysis of the experimental test. Here, the structural behaviour was measured with the load-carrying capacity due to external loading (P_{max}), together with the midspan girder deflections of each girder ($\delta_{i,max}$) and the maximum tendon and stirrup strains ($\varepsilon_{sp,max}$ and $\varepsilon_{sp,max}$) at the load level of 12 MN. This was the load level where the loading procedure was changed. These response variables were investigated based on the concept of fractional factorial design at two levels with resolution III (Box et al. 1978). With this concept, it is generally preferred to use higher resolutions (IV or V) in order to capture interactions between modelling parameters and to avoid main effects cofounded with two-factor interactions. However, due to the high computational effort (i.e., running time in the range of approximately 1.5 day to 15 days), the resolution was reduced in order to limit the required number of runs to 16 and to enable evaluation of up

to 15 modelling variables. Thus, the uncertainty associated with the low level of resolution should be kept in mind in the evaluation of the results from the sensitivity study.

The modelling parameters investigated are listed in Table 5, where level (A) corresponds to the assumptions in the base model and level (B) gives the other extreme to be examined. The majority of the parameters studied were quantitative parameters relating to the material model of concrete. The concrete input parameters, and the basis of their two levels, were defined as follows:

- **Elastic modulus (E_c):** (A) value directly from *in situ* cylinder tests, and (B) value derived according to Model Code 1990 (CEB-FIP 1993) based on *in situ* tested compressive strength.
- **Tensile strength (f_t):** (A) value derived from prior experience (Puurula et al. 2015) based on *in situ* tested compressive strength, and (B) value derived according to Model Code 1990 (CEB-FIP 1993) based on *in situ* tested compressive strength.
- **Compressive strength (f_c):** (A) value directly from *in situ* cylinder tests, and (B) value according to the assessment code (TDOK 2013:0267 2017) for specified concrete quality.
- **Fracture energy (G_f):** (A) value derived from prior experience (Puurula et al. 2015) based on *in situ* tested compressive strength, and (B) value derived according to Model Code 1990 (CEB-FIP 1993) based on *in situ* tested compressive strength.
- **Level of transition from rotated to fixed crack approach (c_{fc}):** (A) lower conservative level suggested by ATENA (2016b), and (B) upper level suggested by ATENA (2016b).
- **Crack band width (L_t):** (A) maximal crack spacing according to the European standard (SS-EN 1992-1-1 2005), or (B) extracted from the crack band approach by the finite element size and crack orientation.
- **Tension stiffening factor (c_{ts}):** (A) lower level suggested by ATENA (2016b) for sparely reinforced regions, and (B) lower level suggested by ATENA (2016b) for relatively dense reinforced regions.
- **Aggregate interlock (denoted a_g):** (A) considered in the constitutive model with the actual aggregate size, and (B) ignored in the constitutive model.

- **Shear stiffness reduction factor (s_F):** (A) conservative level recommended by ATENA (2016b), and (B) alternative level suggested by ATENA (2016b).
- **Limitation of concrete strength reduction factor (r_c^{lim}):** (A) value recommended by Hendriks et al. (2017), and (B) value recommended by ATENA (2016b).

In addition to the concrete parameters, aspects associated with the discretisation by finite elements, residual prestress forces, boundary conditions and the presence of strengthening were also included in the sensitivity study. These parameters are also included in Table 5:

- **Interpolation type within the finite elements:** (A) quadratic interpolation, and (B) linear interpolation.
- **Finite element dimensions (denoted Mesh size in Table 5):** (A) recommended mesh size, as specified in Table 4, and (B) half of the recommended mesh size.
- **Level of the residual prestress forces (denoted ΔP in Table 5):** (A) forces estimated by the standard procedure, and (B) 20 % decrease of the forces estimated by the standard procedure.
- **Boundary conditions at the base of the columns (denoted BC in Table 5):** (A) partially restrained using elastic springs, and (B) freely rotational around all axes.
- **NSM CFRP strengthening of the central girder (denoted Strengthening in Table 5):** (A) strengthening included, and (B) strengthened excluded.

Table 5 illustrates how the response is influenced by changes in the investigated modelling parameters. The modelling parameters are in order of importance for the load-carrying capacity, and the change in response is shown such that the increase (blue) or decrease (red) due to the studied parameters' changes can be compared. Note that the influences of the different parameters shown in Table 5 can only be compared for a certain response variable, while the influence of a given modelling parameter on different response variables cannot be directly compared. This study shows that all the investigated parameters, except for the limitation of the concrete strength reduction factor, are of significance for the analysis of the structural behaviour. However, the importance of different parameters depends on the response variable, with the most influential being the compressive and tensile strength, elastic modulus,

tension stiffening factor, level of residual prestress force, boundary condition assumed at the base of the columns and the presence of NSM CFRP strengthening in the model. All of these most influential parameters, with the exception of the strengthening of the central girder, can also be assumed to be crucial for the failure mode, based on the impact on the measured strains in the tendons and stirrups, respectively. Moreover, it can be concluded that the mesh size dependency is small in relation to the other modelling parameters; this also supports the conclusion made from the separate mesh sensitivity study (see Section 6.3).

The changes of the response variable, when modifying the model parameters from (A) to (B), are generally in the expected direction. For instance, an increased tensile strength or an increased stress level for the transition from rotated to fixed crack approach both increased the load-carrying capacity. Thus, it is possible to conclude that the concrete modelling parameters used in the base model, given by recommended ranges in the nonlinear FE modelling framework, were on the conservative side with regard to the load-carrying capacity. Since it is not easy to carry out *in situ* tests of all the concrete parameters used in the constitutive model (e.g., tension stiffening, level of transition from rotated to fixed crack approach, aggregate interlock and shear stiffness reduction factor), and the analyst has to rely on well-established theories, this kind of information, gained from the sensitivity study, plays an important role in the assessment of existing structures. The concrete properties are usually related to the compressive strength and, as discussed in Section 5.3, this can yield inaccurate estimates of the tensile properties. From Table 5 it is obvious that it is preferable to include *in situ* tests of both the compressive and tensile properties in the assessment, rather than limiting the testing to the compressive strength or just basing it on the theoretical values given by the code. This confirms the findings in the enhanced structural analysis of the experimental test, where representative values of the tensile properties were crucial for the precise prediction of both the load-carrying capacity and failure mode.

In addition to the results shown in Table 5, the sensitivity study showed that the computational effort was greatly affected by the choice of interpolation type and dimensions of finite elements. A change from linear to quadratic interpolation of elements and halved lengths of the element sides,

respectively, yielded an average of more than double the running time to the peak load. Thus, the modelling choices with regard to the finite elements can be an important consideration in the cases of assessment of large structures, where the computational effort becomes critical for the applicability of nonlinear FE analysis. Related to the type of interpolation, there are contradictions in the present guidelines: quadratic interpolation is recommended by Hendriks et al. (2017), and linear interpolation is recommended by the developer of ATENA (2016b) due to the fact that the crack band approach implemented in the software is better suited and, thus, more efficient for this choice. Moreover, the study of the structural behaviour and its sensitivity to different modelling parameters indicated that the mesh size and interpolation type exerted relatively small influences (see Table 5). There is some motivation, therefore, to consider using the less strict, and more efficient, recommendations provided by ATENA (2016b).

7 Conclusions

A strategy for structural analysis on four successively evolved levels (Levels 1 – 4) has been described for evaluating the ultimate load-carrying capacity of the superstructures of concrete bridges. At the initial level, only the action effects are predicted by the structural analysis, while failures related to flexure, shear and anchorage are successively taken into account implicitly at the subsequent levels. This multi-level strategy is proposed as a framework for structural analysis in enhanced assessments, along with other available techniques forming a comprehensive assessment strategy for existing bridges.

In order to evaluate the multi-level structural assessment strategy, results from failure tests of a 55 year-old prestressed concrete girder bridge have been used. From this rare opportunity to examine and calibrate methods applied for determining load-carrying capacities, the following conclusions can be drawn:

- The experimental *in situ* test of the bridge produced highly nonlinear structural behaviour with extensive concrete cracking, yielding of the reinforcing steel and large deformations, thus, providing warning of the imminent failure. A shear-related failure mode took place with

pronounced diagonal cracks in the girder, rupture of the crossing shear reinforcement and also with the loading plate punched through the slab at the top of the girder. The first girder failed with a total external load of 13.4 MN applied to the structure and, with further loading, a similar failure took place in the adjacent girder at 12.8 MN. Thus, a robust and resilient structure was concluded to have considerable residual load-carrying capacity.

- A comparative study between the experimental test and the initial level of structural assessment (i.e., Level 1 of the multi-level strategy), based on the two-step procedure of verification of action effects from structural analysis against sectional resistance given by local models, indicated appreciably conservative estimates of the load-carrying capacity. The estimates was 25 – 68 % of the tested value using linear structural analysis, depending on the shear model applied, and up to 78 % using linear analysis with limited redistribution of internal forces. The shear resistance models, as described by Model Code 2010 (fib 2013) at Level I and European standard (SS-EN 1992-1-1 2005), were not able to predict the location of the shear failure accurately. In contrast, the models described by Model Code at Levels II and III located the failure in line with the test, however, with greatly conservative estimates of the resistance.
- Due to nonlinear behaviour of the bridge and conservatism in the local resistance models, the actual structural behaviour of the bridge can be considered as poorly predicted by the initial level of structural assessment, albeit on the safe side. Consequently, nonlinear FE analysis was recommended for use in a refined assessment. With regard to the critical failure modes indicated by the initial assessment, such an enhanced assessment would preferably be carried out at a level of the multi-level assessment strategy so that both the flexural and the shear response, including associated failure modes, can be precisely and implicitly predicted in the structural analysis (i.e. Level 3 or higher of the multi-level strategy).
- Nonlinear FE analysis involves many modelling choices, and to support these choices a modelling framework based on the general guidelines by Hendriks et al. (2017) and the software-specific recommendations by ATENA (2016a, b) has been briefly described. Despite the guidelines, many

modelling choices remain, which may lead to different outcomes depending on the experience of the analyst. This analyst dependency is undesirable and should be reduced through further improved guidelines. The presented study provides useful information for some crucial aspects associated with the assessment of existing concrete bridges.

- Enhanced structural assessment using nonlinear FE analysis was carried out with a level of detailing such that flexural and shear-related failure modes could be captured (i.e., Level 3 of the multi-level strategy); the defined nonlinear FE modelling framework was strictly followed. The simulation of the experimental test was able to reproduce the actual structural behaviour, identifying the failure mechanism with a predicted load-carrying capacity of 13.9 MN (i.e., a difference to the test of less than 3.8 %). Thus, the enhanced assessment produced highly precise results in relation to the test.
- Simulations of the experimental test showed that relatively small changes in the model produced major changes in the load-carrying capacity and also the failure mechanism. An extensive sensitivity study of the modelling parameters' influence on the structural response was carried out using factorial design. From a range of important modelling parameters, the most influential in this study were the concrete compressive and tensile strength, concrete elastic modulus, tension stiffening, level of residual prestress force, boundary conditions at supports and the consideration of CFRP strengthening applied to one of the tested girders. Thus, it shows the need for representative material properties and boundary conditions to achieve reliable and precise structural assessments of existing bridges (e.g., by following the proposed multi-level strategy). Here, *in situ* investigations are highly recommended for assessing the structure and, with regard to the concrete testing, it should not be limited to just the compressive strength. Moreover, when using nonlinear FE analysis, a sensitivity study can be generally recommended in order to identify crucial uncertainties, the correct modelling of which is of particular importance.
- For investigation of large structures (e.g., bridges), the computational effort required can be enormous and therefore the possibility of using different detailing depending on the structural part

is useful. There is a lack of guidance on this issue. However, this paper provides one example and discussions on how to use reduce the computational effort and how to verify related modelling choices. For instance, a mesh sensitivity study plays an important role in assessment using nonlinear FE analysis.

Based on the full-scale bridge failure, the study shows the advantage of the assessment of existing bridges by using the multi-level structural assessment strategy. Initial assessment yielded very conservative predictions, but enhanced levels of analysis have the capability to predict the structural behaviour and load-carrying capacity accurately, even for complex problems. Nevertheless, to avoid misleading conclusions, uncertainties in the analysis should be systematically accounted for by, for instance, using modelling guidelines and bridge-specific data.

Acknowledgements

The authors would like to acknowledge the financial support of Swedish Transport Administration (Trafikverket), Program for Research and Innovation for Civil Structures in the Transport Sector (BBT), Luossavaara-Kiirunavaara AB (LKAB), Hjalmar Lundbohm Research Center (HLRC), Development Fund of the Swedish Construction Industry (SBUF), ÅForsk Foundation, Norut Northern Research Institute and Luleå University of Technology (LTU). They also thank colleagues in the Swedish Universities of the Built Environment (CTH, KTH, LTH and LTU) for fruitful collaboration during the project. The experimental work was carried out in cooperation with Complab at LTU, whose expertise was essential for success of the tests.

References

ABAQUS (2012). *Abaqus theory manual*. Providence, RI, United States: SIMULIA.

ACI 318 (2014). *Building code requirements for structural concrete and commentary*. Farmington Hills, MI, United States: American Concrete Institute (ACI).

Aktan, A. E., Zwick, M., Miller, R., & Shahrooz, B. (1992). Nondestructive and destructive testing of decommissioned reinforced concrete slab highway bridge and associated analytical studies. *Transportation Research Record* (1371), 142-153.

ANSYS (2013). *ANSYS mechanical APDL theory reference* (Release 15.0). Swanson Analysis Systems.

ATENA (2016a). *ATENA program documentation - Part 11: Troubleshooting manual*. Prague, Czech Republic: Červenka Consulting.

ATENA (2016b). *ATENA program documentation - Part 1: Theory*. Prague, Czech Republic: Červenka Consulting.

Azizinamini, A., Boothby, T., Shekar, Y., & Barnhill, G. (1994). Old concrete slab bridges. I: Experimental investigation. *Journal of Structural Engineering*, 120(11), 3284-3304.

Bagge, N., Nilimaa, J., Blanksvärd, T., & Elfgren, L. (2014). Instrumentation and full-scale test of a post-tensioned concrete bridge. *Nordic Concrete Research*, 51, 63-83.

Bagge, N., Nilimaa, J., Enochsson, O., Sabourova, N., Grip, N., Emborg, M., & Elfgren, L. (2015a). *Protecting a five span prestressed bridge against ground deformations*. IABSE Conference – Structural Engineering: Providing Solutions to Global Challenges, International Association for Bridge and Structural Engineering (IABSE), Geneva, Switzerland, pp. 255-262.

Bagge, N., Shu, J., Plos, M., & Elfgren, L. (2015b). *Punching capacity of a reinforced concrete bridge deck slab loaded to failure*. Nordic Concrete Research: Residual Capacity of Deteriorated Concrete Structures, Norsk Betongförening Oslo, Norway, 57-60.

Bagge, N., Nilimaa, J., & Elfgren, L. (2017). In-situ methods to determine residual prestress forces in concrete bridges. *Engineering Structures*, 135, 41-52.

Bagge, N., Popescu, C., & Elfgren, L. (2018). Failure tests on concrete bridges: Have we learnt the lessons? *Structure and Infrastructure Engineering*, 14(3), 292-319.

Bažant, Z. P., & Oh, B. H. (1983). Crack band theory for fracture of concrete. *Matériaux et construction*, 16(3), 155-177.

BBK 94 (1994). *Boverkets handbok om betongkonstruktioner. Band 1: Konstruktion* (*Boverket's handbook for concrete structures. Part 1: Design*. In Swedish). Karlskrona, Sweden: Boverket.

Belletti, B., Damoni, C., den Uijl, J. A., Hendriks, M. A. N., & Walraven, J. C. (2013). Shear resistance evaluation of prestressed concrete bridge beams: fib Model Code 2010 guidelines for level IV approximations. *Structural Concrete*, 14(3), 242-249.

Bentz, E. C., & Collins, M. P. (2006). Development of the 2004 Canadian Standards Association (CSA) A23.3 shear provisions for reinforced concrete. *Canadian Journal of Civil Engineering*, 33(5), 521-534.

Bentz, E. C., Vecchio, F. J., & Collins, M. P. (2006). Simplified modified compression field theory for calculating shear strength of reinforced concrete elements. *ACI Structural Journal*, 103(4), 614-624.

Bigaj, A. J. (1999). *Structural dependence of rotations capacity of plastic hinges in RC beams and slabs*. Ph.D. Thesis, Delft University of Technology, Delft, Netherlands.

Bocchini, P., Frangopol, D. M., Ummenhofer, T., & Zinke, T. (2013). Resilience and sustainability of civil infrastructure: Toward a unified approach. *Journal of Infrastructure Systems*, 20(2), 1-16.

Box, G. E. P., Hunter, W. G., & Hunter, J. S. (1978). *Statistics for experimenters: An introduction to design, data analysis, and model building*, New York, NY, United States: John Wiley & Sons.

BRIME (2001). *Bridge management in Europe* (Final report). Brussels, Belgium: Bridge Management in Europe (BRIME) – 4th Framework Programme.

Broo, H., Plos, M., Lundgren, K., & Engström, B. (2007). Simulation of shear-type cracking and failure with non-linear finite-element method. *Magazine of Concrete Research*, 59(9), 673-687.

Broo, H., Lundgren, K., & Plos, M. (2008). *A guide to non-linear finite element modelling of shear and torsion in concrete bridges* (Report 2008:18). Gothenburg, Sweden: Chalmers University of Technology.

Broo, H., Plos, M., Lundgren, K., & Engström, B. (2009). Non-linear finite-element analysis of the shear response in prestressed concrete bridges. *Magazine of Concrete Research*, 61(8), 591-608.

Burdette, E. G., & Goodpasture, D. W. (1971). *Full-scale bridge testing: An evaluation of bridge design criteria*. Knoxville, TN, United States: University of Tennessee.

CEB-FIP (1993). *CEB-FIP Model Code 1990*, London, United Kingdom: Thomas Telford Ltd.

CEB (1998). *Ductility of reinforced concrete structures* (Bulletin 242*)*. Lausanne, Switzerland: Comité Euro-International du Béton (CEB).

Červenka, J., & Papanikolaou, V. K. (2008). Three dimensional combined fracture–plastic material model for concrete. *International Journal of Plasticity*, 24(12), 2192-2220.

Červenka, V., Pukl, R., Ozbolt, J., & Eligehausen, R. (1995). *Mesh sensitivity effects in smeared finite element analysis of concrete fracture*. FraMCoS-2, International Association of Fracture Mechanics for Concrete and Concrete Structures Zurich, Switzerland, pp. 1387-1396.

Cladera, A., & Marí, A. R. (2007). Shear strength in the new Eurocode 2. A step forward? *Structural Concrete*, 8(2), 57-66.

COST-345 (2004). *Procedures required for the assessment of highway structures* (Final report*)*. Brussels, Belgium: Cooperation in the field of scientific and technical research (COST).

CSA A23.3 (2014). *Design of concrete structures*. Rexdale, ON, Canada: Canadian Standards Association (CSA).

de Borst, R. (1986). *Non-linear analysis of frictional materials*. Ph.D. Thesis, Delft University of Technology, Delft, Netherlands.

DIANA (2015). *DIANA finite element analysis* (User's manual release 10.0*)*. Delft, Netherlands: TNO Diana BV.

Dutta, S. C., & Roy, R. (2002). A critical review on idealization and modeling for interaction among soil–foundation–structure system. *Computers & Structures*, 80(20), 1579-1594.

Dyngeland, T. (1989). *Behavior of reinforced concrete panels*. Ph.D. Thesis, Trondheim University, Trondheim, Norway.

Ellingwood, B. R., & Lee, J. Y. (2016). Life cycle performance goals for civil infrastructure: intergenerational risk-informed decisions. *Structure and Infrastructure Engineering*, 12(7), 822-829.

Enochsson, O., Sabourova, N., Emborg, M., & Elfgren, L. (2011). *Gruvvägsbron i Kiruna: Deformationskapacitet* (*The Mine Bridge in Kiruna: Deformation capacity*) (In Swedish), Luleå, Sweden: Luleå University of Technology.

Ferreira, D., Bairán, J., & Marí, A. (2015). Efficient 1D model for blind assessment of existing bridges: simulation of a full-scale loading test and comparison with higher order continuum models. *Structure and Infrastructure Engineering*, 11(10), 1383-1397.

fib (2008). *Practitioners' guide to finite element modelling* (Bulletin 45). Lausanne, Switzerland: International Federation for Structural Concrete (fib).

fib (2013). *fib Model Code for concrete structures 2010*. Berlin, Germany: Ernst & Sohn.

Frangopol, D. M., & Soliman, M. (2016). Life-cycle of structural systems: recent achievements and future directions. *Structure and Infrastructure Engineering*, 12(1), 1-20.

Hanjari, K. Z., Kettil, P., & Lundgren, K. (2011). Analysis of mechanical behavior of corroded reinforced concrete structures. *ACI Structural Journal*, 108(5), 532-541.

Hanjari, K. Z., Kettil, P., & Lundgren, K. (2013). Modelling the structural behaviour of frost-damaged reinforced concrete structures. *Structure and Infrastructure Engineering*, 9(5), 416-431.

Haritos, N., Hira, A., Mendis, P., Heywood, R., & Giufre, A. (2000). Load testing to collapse limit state of Barr Creek Bridge. *Transportation Research Record*, 2, 92-102.

Hendriks, M. A. N., den Uijl, J. A., de Boer, A., Feenstra, P. H., Belletti, B., & Damoni, C. (2012). *Guidelines for nonlinear finite element analysis of concrete structures* (Report RTD: 1016:2012). Rijkswaterstaat Centre for Infrastructure.

Hendriks, M. A. N., de Boer, A., & Belletti, B. (2016). *Guidelines for nonlinear finite element analysis of concrete structures* (Report RTD: 1016-1:2016). Rijkswaterstaat Centre for Infrastructure.

Hendriks, M. A. N., de Boer, A., & Belletti, B. (2017). *Guidelines for nonlinear finite element analysis of concrete structures* (Report RTD: 1016-1:2017). Rijkswaterstaat Centre for Infrastructure.

Hordijk, D. A. (1991). *Local approach to fatigue of concrete*. Ph.D. Thesis, Delft University of Technology, Delft, Netherlands.

Huria, V., Lee, K.-L., & Aktan, A. E. (1993). Nonlinear finite element analysis of RC slab bridge. *Journal of Structural Engineering*, 119(1), 88-107.

Isaksen, H. R., Kanstad, T., Olsen, P.-E., & Giæver, N. A. (1998). *Prøvebelastning av bru nr 02-1234 Smedstua bru: Forutsetninger, gjennomføring og måledata* (*Load test of bridge no 02-1234 Smedstua Bridge: Conditions, execution and measurements*. In Norwegian). Statens Vegvesen.

ISO 2394 (2015). *General principles on reliability of structures*. International Organization for Standardization (ISO).

Kollegger, J., & Mehlhorn, G. (1988). *Experimentelle und Analytische Untersuchungen zur Aufstellung eines Materialmodels fuer Gerissene Stahbetonscheiben* (*Experimental and analytical investigations for development of a material model for cracked concrete slabs*. In German) (Nr. 6 Forschungsbericht). Kasel, Germany: Gesamthochschule Kassel.

MAINLINE (2013). *Benchmark of new technologies to extend the life of eldery rail infrastructure* (Devliverable D1.1). Luleå, Sweden: MAINLINE.

Menetrey, P., & Willam, K. J. (1995). Triaxial failure criterion for concrete and its generalization. *ACI Structural Journal*, 92(3), 311-318.

Mohr, S., Bairán, J. M., & Marí, A. R. (2010). A frame element model for the analysis of reinforced concrete structures under shear and bending. *Engineering Structures*, 32(12), 3936-3954.

Nielsen, M. P., & Hoang, L. C. (2010). *Limit analysis and concrete plasticity*. Boca Raton, FL, United States: CRC Press.

Nilimaa, J. (2015). *Concrete bridges: Improved load capacity*. Ph.D. Thesis, Luleå University of Technology, Luleå, Sweden.

Nilimaa, J., Bagge, N., Blanksvärd, T., & Täljsten, B. (2015). NSM CFRP strengthening and failure loading of a post-tensioned concrete bridge. *Journal of Composites for Construction*, 20(3), 04015076, 2015.

Oreskes, N., Shrader-Frechette, K., & Belitz, K. (1994). Verification, validation, and confirmation of numerical models in the earth sciences. *Science*, 263(5147), 641-646.

Pacoste, C., Plos, M., & Johansson, M. (2012). *Recommendations for finite element analysis for the design of reinforced concrete slabs* (TRITA-BKN Report 144). Stockholm, Sweden: Royal Institute of Technology (KTH).

Pedersen, E. S., Nielsen, P. M., & Lyngberg, B. S. (1980). Investigation and failure test of a prestressed concrete bridge. *IABSE Congress Report*, 11, 849-854.

Plos, M. *Improved bridge assessment using non-linear finite element analyses*. 1st International Conference on Bridge Maintenance, Safety and Management (IABMAS), pp. 133-134.

Plos, M., & Gylltoft, K. (2006). Evaluation of shear capacity of a prestressed concrete box girder bridge using non-linear FEM. *Structural Engineering International*, 16(3), 213-221.

Plos, M., Gylltoft, K., & Cederwall, K. (1990). Full scale shear tests on modern highway concrete bridges. *Nordic Concrete Research*, 9, 134-144.

Plos, M., Shu, J., Zandi, K. Z., & Lundgren, K. (2017). A multi-level structural assessment strategy for reinforced concrete bridge deck slabs. *Structure and Infrastructure Engineering*, 13(2), 223-241.

Pressley, J. S., Candy, C. C. E., Walton, B. L., & Sanjayan, J. G. (2004*). Destructive load testing of bridge no. 1049 – analyses, predictions and testing*. 5th Austroads Bridge Conference, Austroads, Sydney, Australia, 1-12.

Puurula, A. M., Enochsson, O., Sas, G., Blanksvärd, T., Ohlsson, U., Bernspång, L., Täljsten, B., Carolin, A., Paulsson, B., & Elfgren, L. (2015). Assessment of the strengthening of an RC railway bridge with CFRP utilizing a full-scale failure test and finite-element analysis. *Journal of Structural Engineering*, 141(1), 1-11.

Riks, E. (1970). *On the numerical solution of snapping problems in the theory of elastic stability*. Stanford, CA, United States: Stanford University.

Rombach, G. A. (2011). *Finite element design of concrete structures: practical problems and their solution*. London, United Kingdom: ICE Publishing.

Rots, J. G. (1988). *Computational modeling of concrete fracture*. Ph.D. Thesis, Delft University of Technology, Delft, Netherlands.

SAMARIS (2006). *State of the art report on assessment of structures in selected EEA and CE countries* (Deliverable D19). Brussels, Belgium: Sustainable and Advanced Material for Road InfraStructure (SAMARIS).

SB-LRA (2007). *Guideline for load and resistance assessment of existing European railway bridges: Advises on the use of advanced methods*. Luleå, Sweden: Sustainable Bridges.

SB (2007a). *Guideline for Load and Resistance Assessment of Existing European Railway Bridges* (Deliverable 4.2). Brussels, Belgium: Sustainable Bridges (SB) – Assessment for Future Traffic Demands and Longer Lives.

SB (2007b). *Sustainable Bridges - Assessment for future traffic demands and longer lives*. Wrocław, Poland: Dolnośląskie Wydawnictwo Edukacyjne.

Schlune, H. (2011). *Safety evaluation of concrete structures with nonlinear analysis*. Ph.D. Thesis, Chalmers University of Technology, Gothenburg, Sweden.

Schneider, J., & Vrouwenvelder, T. (2017). *Introduction to safety and reliability of structures*. Zürich, Switzerland: International Association for Bridge and Structural Engineering (IABSE).

Šomodíková, M., Lehký, D., Doležel, J., & Novák, D. (2016). Modeling of degradation processes in concrete: Probabilistic lifetime and load-bearing capacity assessment of existing reinforced concrete bridges. *Engineering Structures*, 119, 49-60.

SS-EN 1992-1-1 (2005). *Eurocode 2: Design of concrete structures – Part 1-1: General rules and rules for buildings*. Brussels, Belgium: European Committee for Standardization (CEN).

SS-EN 12390-3 (2009). *Testing hardened concrete – Part 3: Compressive strength of test specimens*. Brussels, Belgium: European Committee for Standardization (CEN).

SS-EN 12390-13 (2013). *Testing hardened concrete – Part 13: Determination of secant modulus of elasticity in compression*. Brussels, Belgium: European Committee for Standardization (CEN).

SS-EN 12504-1 (2009). *Testing concrete in structures – Part 1: Cored specimens – Taking, examining and testing in compression*. Brussels, Belgium: European Committee for Standardization (CEN).

SS-EN ISO 6892-1 (2009). *Metallic materials – Tensile testing – Part 1: Method of test at room temperature*. Brussels, Belgium: European Committee for Standardization (CEN).

SS-EN ISO 15630-1 (2010). *Steel for the reinforcement and prestressing of concrete – Test methods – Part 1: Reinforcing bars, wire rod and wire*. Brussels, Belgium: European Committee for Standardization (CEN).

SS-EN ISO 15630-3 (2010). *Steel for the reinforcement and prestressing of concrete – Test methods – Part 3: Prestressing steel*. Brussels, Belgium: European Committee for Standardization (CEN).

Strängbetong (n.d.). BBRV spennarmering (BBRV prestressed reinforcement. In Norwegian). Oslo, Norway: AS Strängbetong.

Tahershamsi, M., Fernandez, I., Zandi, K., & Lundgren, K. (2017). Four levels to assess anchorage capacity of corroded reinforcement in concrete. *Engineering Structures*, 147, 434-447.

TDOK 2013:0267 (2017). *Bärighetsberäkning av broar: Krav* (*Structural assessment of bridges: Requirements*. In Swedish) (Version 4.0). Borlänge, Sweden: Trafikverket.

Thun, H., Ohlsson, U., & Elfgren, L. (1999). *Betonghållfasthet i järnvägsbroar på Malmbanan: Karakteristisk tryck- och draghållfasthet för 20 broar mellan Luleå - Gällivare* (*Concrete Strength in Railway Bridges along Malmbanan: Characteristic Compression and Tensile Strength for 20 bridges between Luleå and Gällivare*. In Swedish). Luleå, Sweden: Luleå University of Technology.

Thun, H., Ohlsson, U., & Elfgren, L. (2006). Concrete strength in old Swedish concrete bridges. *Nordic Concrete Research*, 35(1-2), 47-60.

Thurlimann, B. (1979). Shear strength of reinforced and prestressed concrete-CEB approach. *Special Publication*, 59, 93-116.

U.S. Department of Transportation (2016). *Transportation in the United States: Highlights from 2015 transportation statistics annual report*. Washington, DC, United States: U.S. Department of Transportation, Bureau of Transportation Statistics.

UIC 778-4R (2009). *Defects in railway bridges and procedures for maintenance*. Paris, France: International Union of Railways (UIC).

Walraven, J. C. (1981). Fundamental analysis of aggregate interlock. *Journal of the Structural Division*, 107(11), 2245-2270.

van Mier, J. G. (1986). Multiaxial strain-softening of concrete. *Materials and Structures*, 19(3), 190-200.

Vecchio, F. J., & Collins, M. P. (1986). The modified compression-field theory for reinforced concrete elements subjected to shear. *ACI Journal*, 83(2), 219-231.

Weder, C. (1977). *Die vorgespannte, zwanzigjährige Stahlbetonbrücke über die alte Glatt bei Schwamendingen, Zürich* (*Prestressed, twenty year-old RC bridge over the old Glatt at Schwamendingen, Zürich*. In German) (Report no. 203). Swiss Federal Laboratories for Materials Science and Technology (EMPA).

Wempner, G. A. (1971). Discrete approximations related to nonlinear theories of solids. *International Journal of Solids and Structures*, 7(11), 1581-1599.

Ypma, T. J. (1995). Historical development of the Newton-Raphson method. *SIAM Review*, 37(4), 531-551.

Table 1. Concrete properties.

Quality class	Design		Assessment		*In situ*	
	f_{ck}	E_{ck}	$f_{ck,upgr}$	$E_{ck,upgr}$	$f_{cm,is}$ (CoV)	$E_{cm,is}$ (CoV)
	MPa	GPa	MPa	GPa	MPa	GPa
K300	21.5	30.0	32.0	33.0	61.8 (11 %)	32.4 (6.8 %)
K400	28.5	32.0	35.5	34.0	62.3 (18 %)	32.0 (8.9 %)
All	-	-	-	-	62.2 (16 %)	32.1 (8.3 %)

Table 2. Reinforcing steel properties.

Quality class	ϕ	Design and assessment			*In situ*		
		f_{yk}[a)]	f_{tk}	ε_{uk}	$f_{ym,is}$[b)] (CoV)	$f_{tm,is}$ (CoV)	$\varepsilon_{um,is}$ (CoV)
	mm	MPa	MPa	%	MPa	MPa	%
St145/170	6	1450	1700	3.5	1606 (1.4 %)	1734 (0.9 %)	4.7 (5.1 %)
Ks40	10	410	600	16	484 (5.8 %)	702 (2.9 %)	13 (12 %)
Ks40	16	410	600	16	439 (2.3 %)	705 (1.5 %)	13 (4.9 %)
Ks40	25	390	600	16	389 (4.3 %)	629 (3.3 %)	14 (9.2 %)
Ks60	10	620	750	12	679 (5.0 %)	1000 (1.7 %)	10 (5.5 %)
Ks60	16	620	750	12	584 (2.2 %)	831 (2.4 %)	11 (5.3 %)

[a)] $f_{p0.2k}$ for quality class St145/170
[b)] $f_{p0.2m,is}$ for quality class St145/170

Table 3. Maximal dimensions of quadratic continuum finite elements along the main directions of typical structural elements, from Hendriks et al. (2017).

Model idealisation	Beam			Slab		
	Length	Height	Width	Length	Height	Width
2D	$l/50$	$h/6$	-	$l/50$	-	$b/50$
3D	$l/50$	$h/6$	$b/6$	$l/50$	$h/6$	$b/50$

Table 4. Finite element types and maximal element sizes (or number of cells in the height and width directions of beam elements and number of layers in the height direction of shell elements) in the bridge's global directions.

Structural element	Material idealisation	Element type	Element size in bridge global directions		
			Longitudinal	Vertical	Transverse
Foundation	Linear	Shell	4 layers	≤ 2.0 m	≤ 2.0 m
Column	Linear	Beam	4 cells	≤ 1.0 m	4 cells
Girder	Linear	Beam	≤ 2.0 m	4 cells	2 cells
Slab	Linear	Shell	≤ 2.0 m	4 layers	≤ 2.0 m
Curb	Linear	Beam	≤ 2.0 m	4 cells	4 cells
Cross-beam	Linear	Beam	2 cells	4 cells	≤ 1.0 m
Girder	Nonlinear	Continuum	≤ 0.40 m	6 el. (≤ 0.27 m)	2 el. (≤ 0.33 m)
Slab	Nonlinear	Shell	≤ 0.40 m	4 layers	≤ 0.40 m
Curb	Nonlinear	Beam	≤ 0.40 m	4 cells	4 cells
Cross-beam	Nonlinear	Continuum	1 el. (≤ 0.40 m)	6 el. (≤ 0.27 m)	≤ 0.40 m
Slab [a)]	Nonlinear	Continuum	≤ 0.15 m	6 el. (≤ 0.05 m)	≤ 0.15 m
Flange [b)]	Linear	Shell	4 el. (≤ 0.17 m)	2 layers	20 el. (≤ 0.26 m)
Web [b)]	Linear	Shell	2 layers	6 el. (≤ 0.19 m)	20 el. (≤ 0.26 m)
Stiffener [b)]	Linear	Shell	1 el. (≤ 0.17 m)	6 el. (≤ 0.19 m)	2 layers
Loading plates [b)]	Linear	Shell	4 el. (≤ 0.17 m)	2 layers	4 el. (≤ 0.17 m)

[a)] locally refined region at load application (see Figure 6(b))
[b)] load distribution beams

Table 5. Sensitivity study of the bridge externally loaded to failure with the response variables being the load-carrying capacity (P_{max}) and the maximal deflections of each girder ($\delta_{i,max}$) and the tendon ($\varepsilon_{sp,max}$) and the stirrup strain ($\varepsilon_{sw,max}$) for the most strained reinforcement unit at the load level of 12 MN.

Modelling parameter	Levels [a]		Response variables [b]					
	A	B	P_{max} MN	$\delta_{S,max}$ mm	$\delta_{C,max}$ mm	$\delta_{N,max}$ mm	$\varepsilon_{sp,max}$ ‰	$\varepsilon_{sw,max}$ ‰
c_{ts}	0.01	0.10						
f_t	2.00 MPa	4.30 MPa						
c_{fc}	0.60	0.90						
a_g	32 mm	-						
s_F	20	200						
G_f	140 N/m	208 N/m						
Interpolation	Quadratic	Linear						
r_c^{lim}	0.40	0.80						
Mesh size	Recommended	Reduced (½)						
E_c	32.1 MPa	39.5 MPa						
ΔP	0	- 20 %						
BC	Spring	Hinge						
L_t	200 mm	-						
f_c	- 62.2 MPa	- 35.5 MPa						
Strengthening	CFRP	-						

[a] (A) specifies assumed modelling parameter in the base model, and (B) specifies alternative modelling parameter in the sensitivity study

[b] red colour indicates decreased value when a factor goes from (A) to (B), and blue colour indicates increased value when a factor goes from (A) to (B)

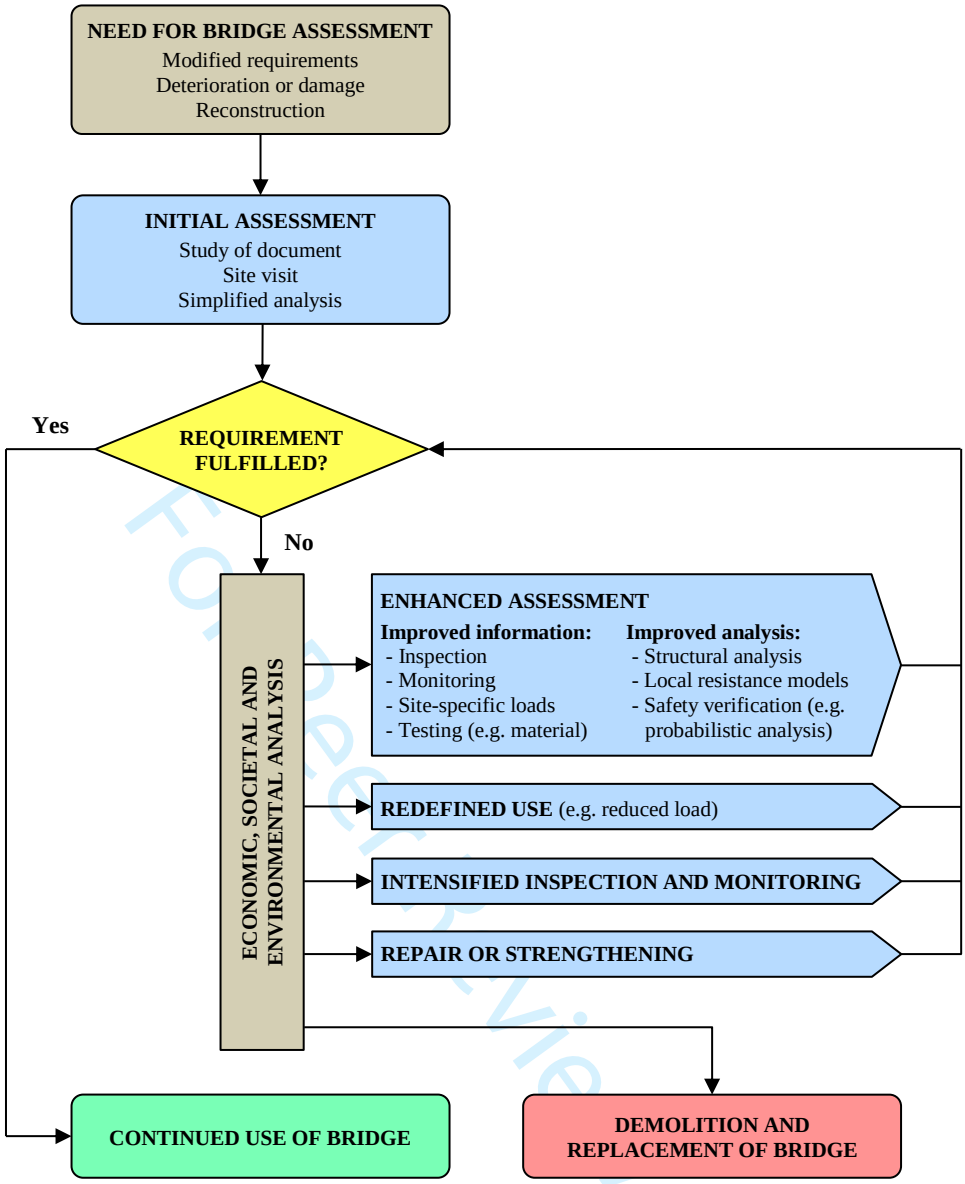

Figure 1. Bridge assessment approach.

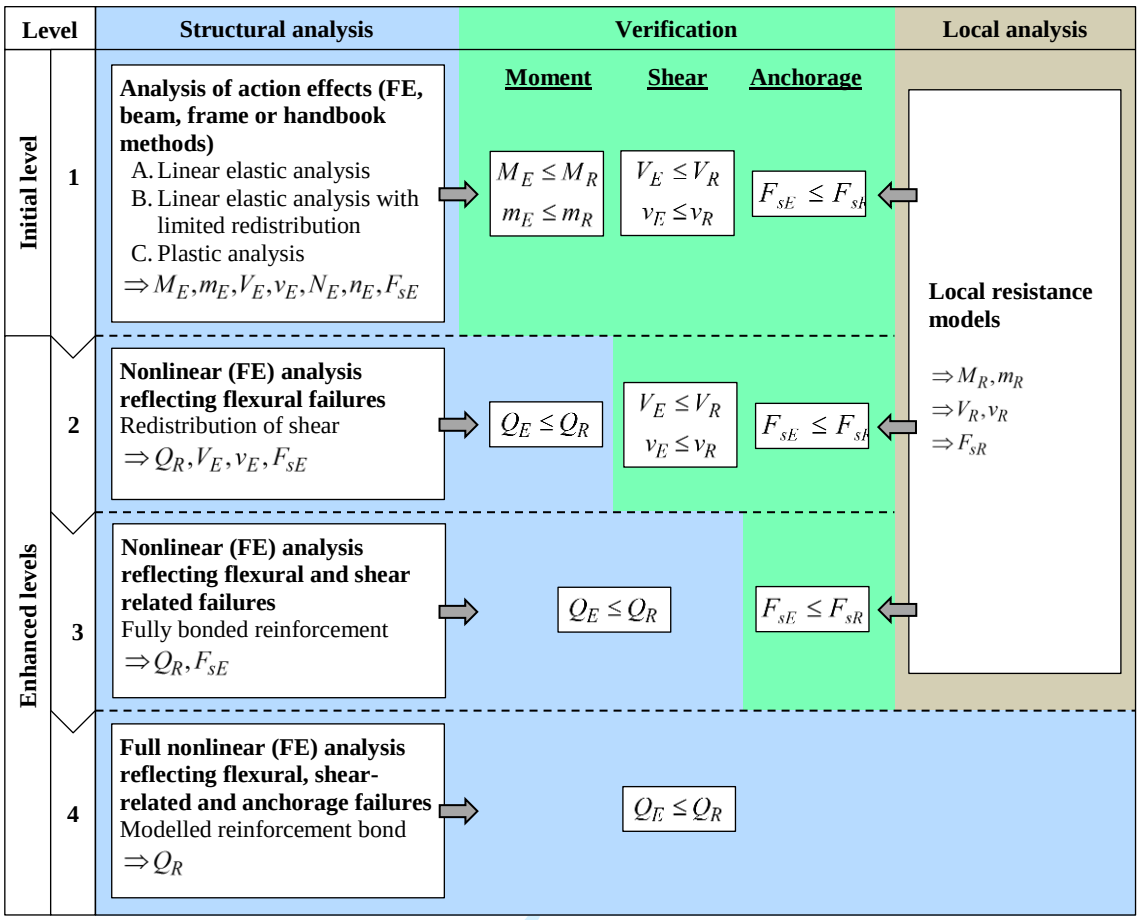

Figure 2. Multi-level strategy for structural analysis of superstructures of concrete bridges.

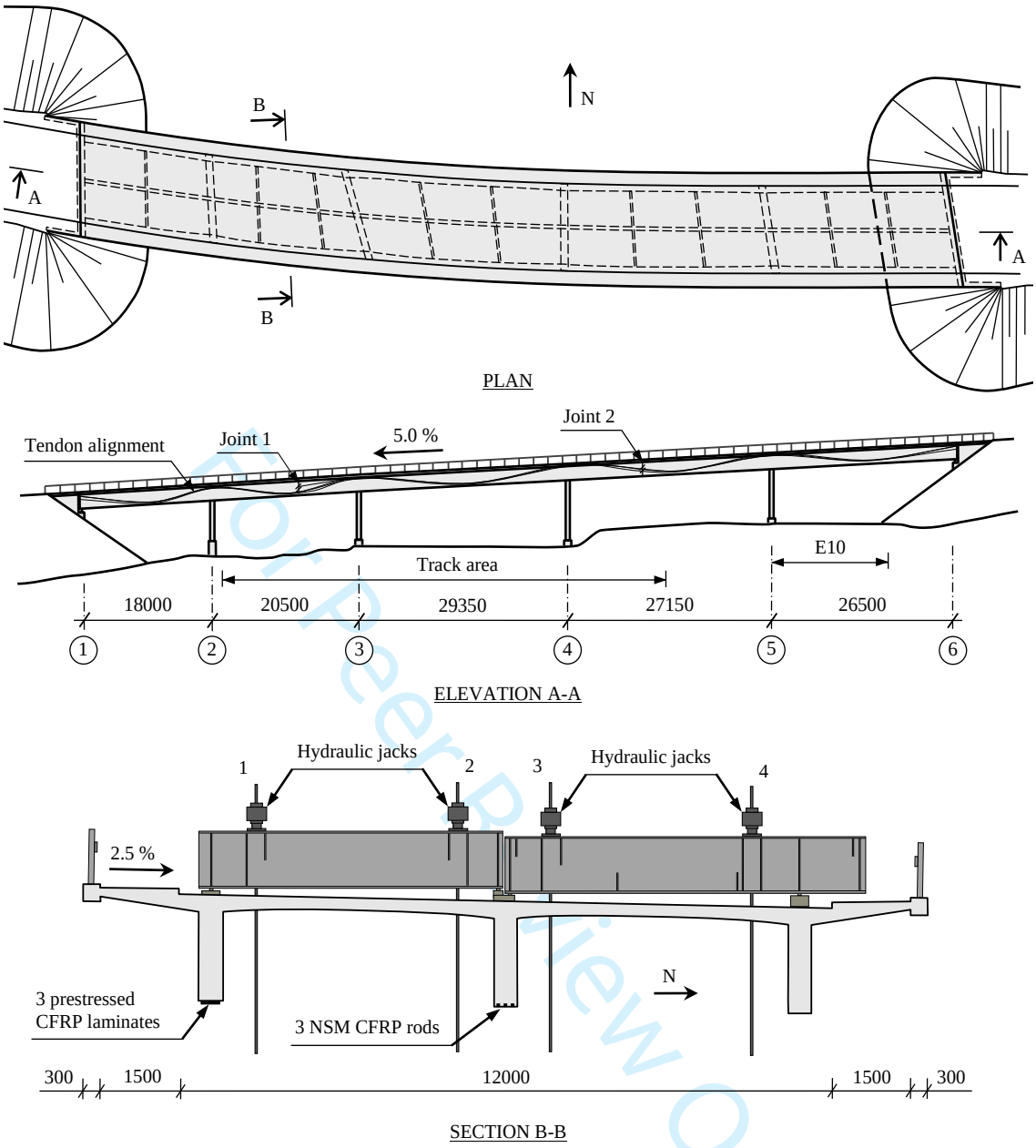

Figure 3. Bridge geometry and test setup (measurements in mm).

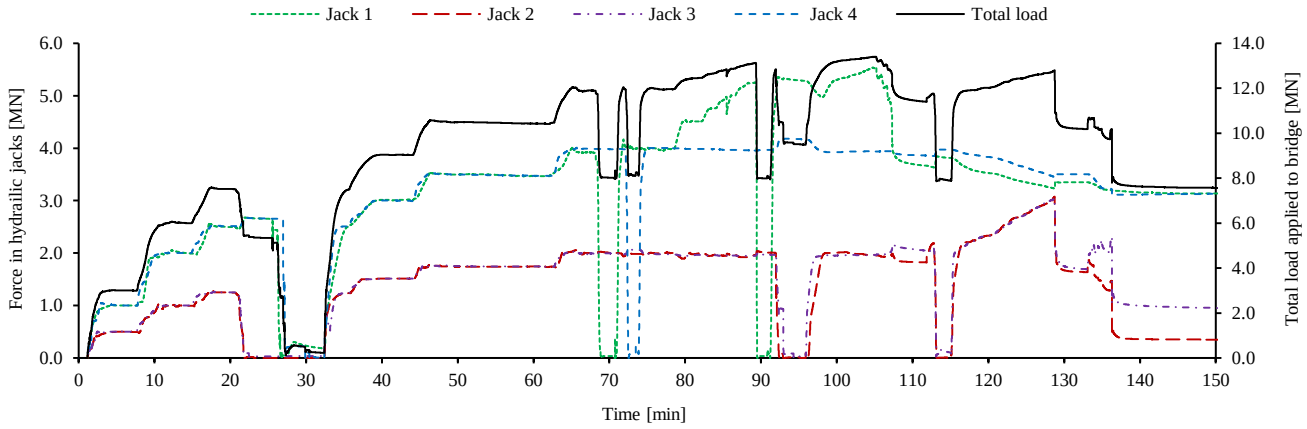

Figure 4. Loading schedule of the bridge failure test.

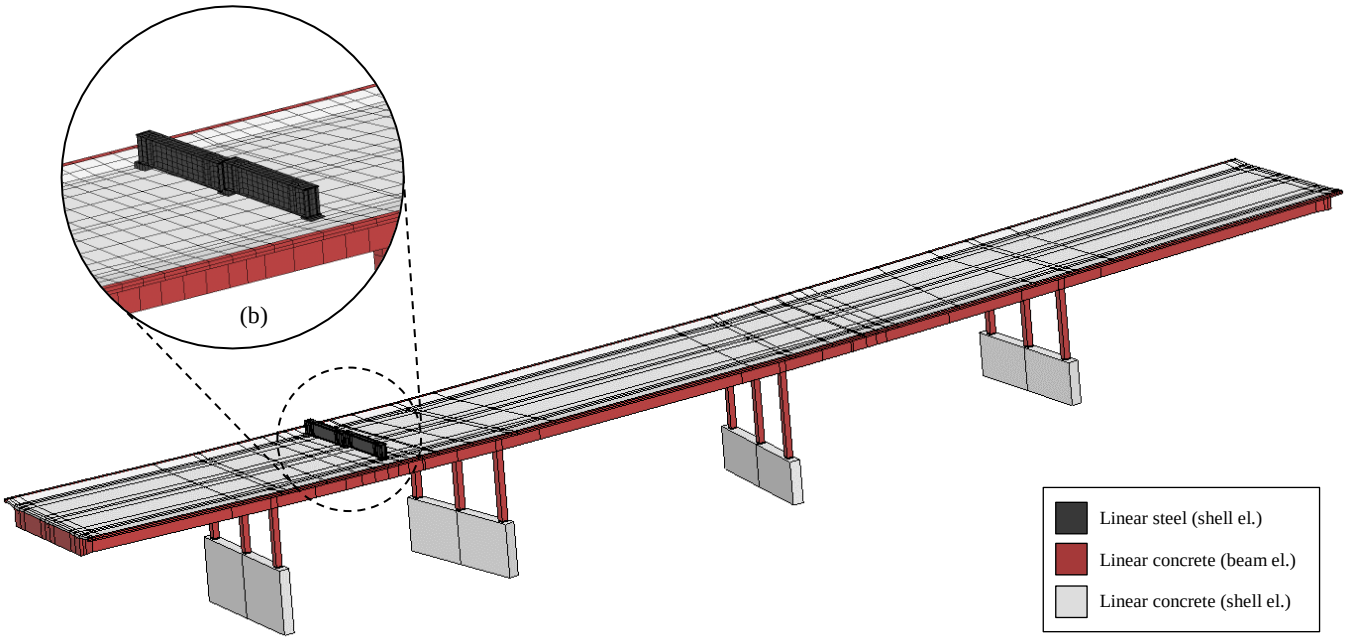

(a)

Figure 5. Finite element model of bridge: (a) geometry and discretisation with different types of finite elements and (b) load distribution beam and visualisation of finite elements.

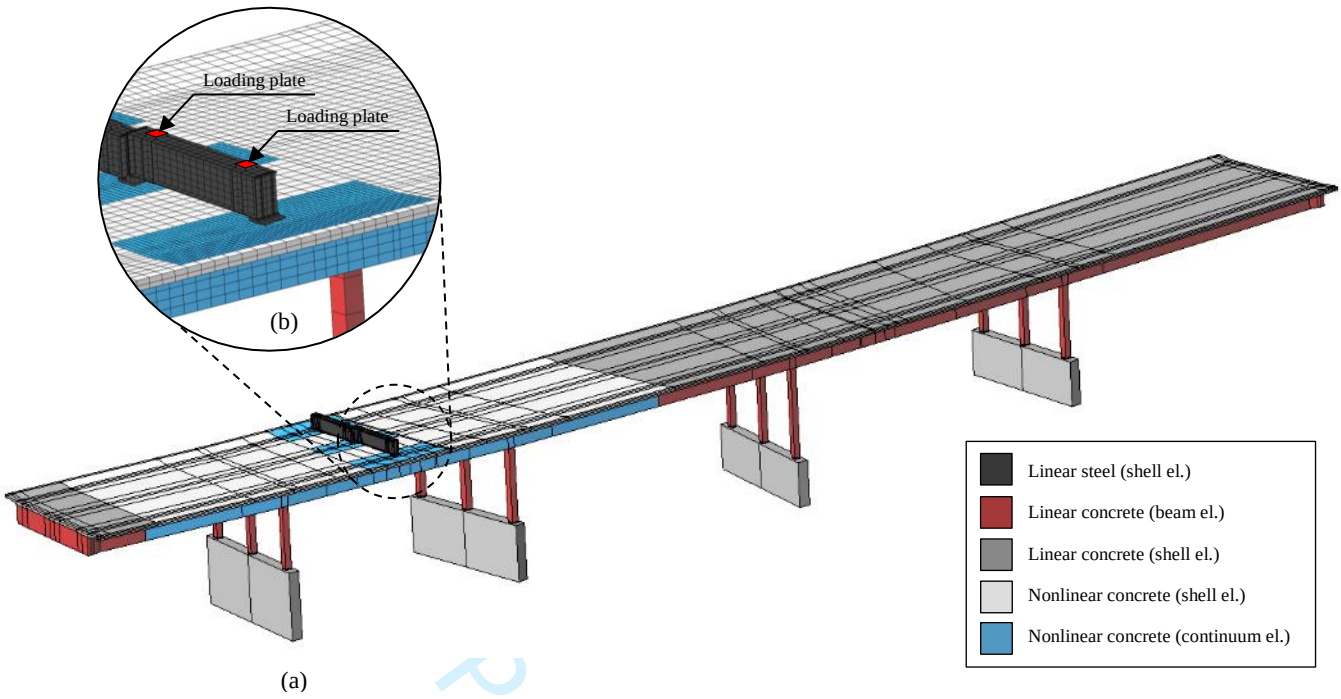

Figure 6. Finite element model of bridge: (a) geometry and discretisation with different types of finite elements, (b) load distribution beam and visualisation of finite elements at refined region of the bridge deck slab above the south girder.

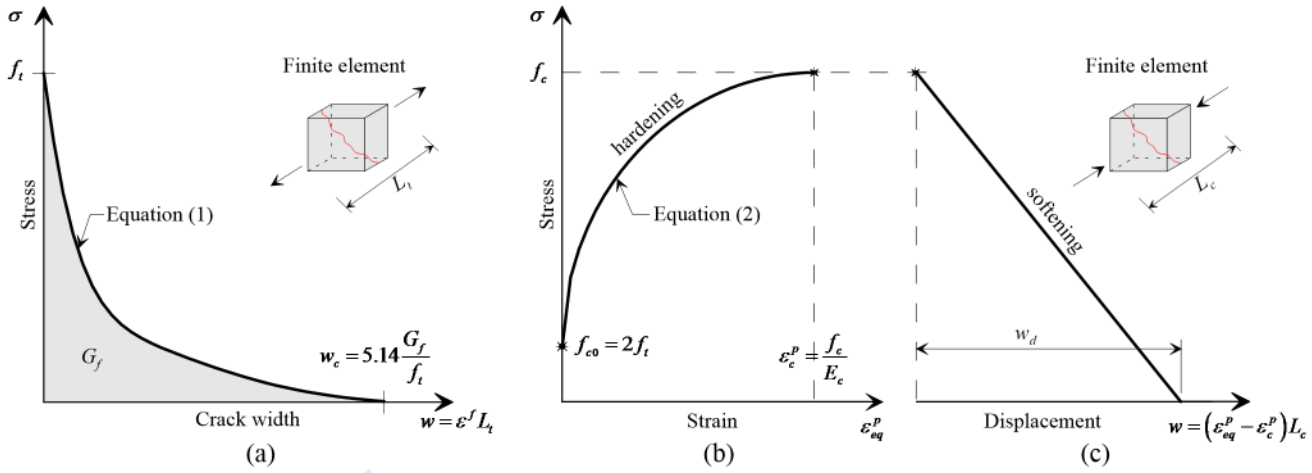

Figure 7. Uniaxial response according to the concrete constitutive model used: (a) stress-displacement relationship for softening in tension, (b) stress-strain relationship for hardening in compression, and (c) stress-displacement relationship for softening in compression.

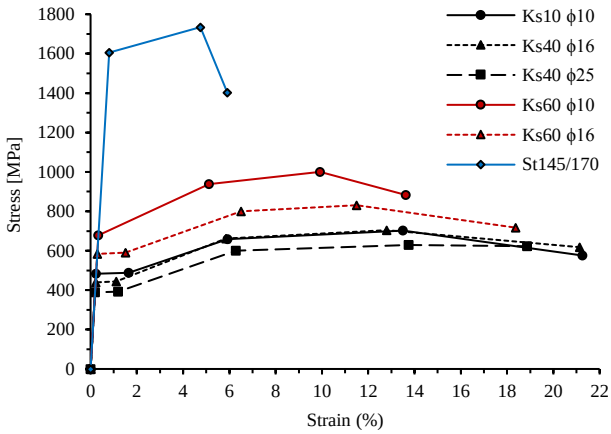

Figure 8. Multi-linear stress-strain relationships of reinforcing steel used in FE model.

(a)

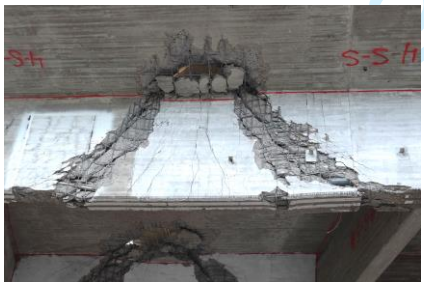

(b)

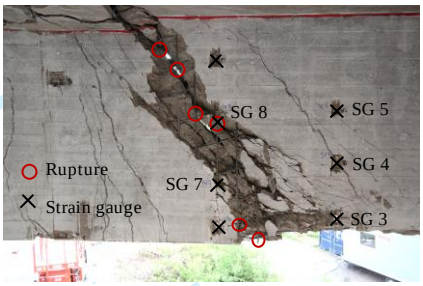

(c)

(d)

Figure 9. Bridge girders loaded to failure: (a) span 2 subjected to external loads centrically over the girders at midspan, view from south, (b) failure of south girder, view from south, (c) diagonal concrete cracking, stirrup ruptures and positions of strain gauges (SG) attached to stirrups on the south girder, view from north, and (d) failure of bridge deck slab, view from above. (Images by Niklas Bagge).

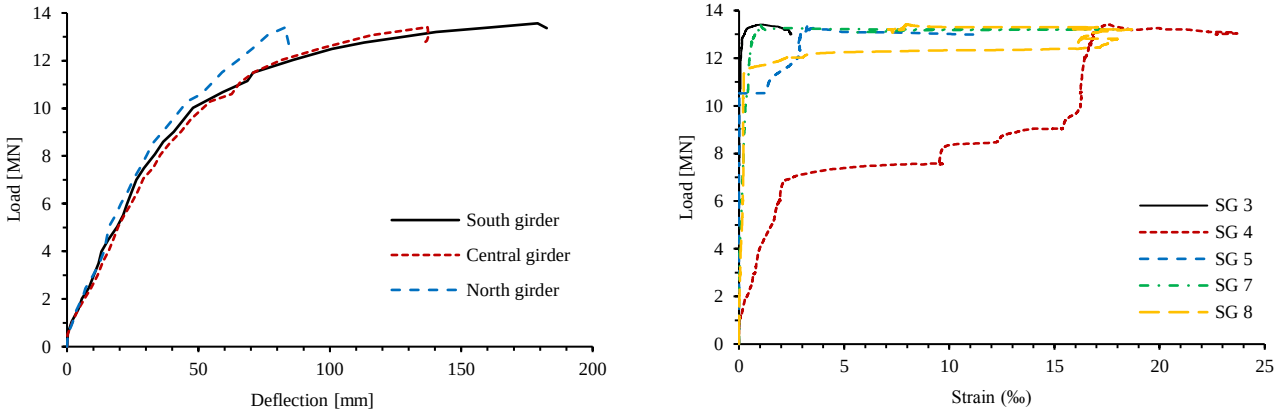

(a) (b)

Figure 10. Measurements during the failure test of the south bridge girder: (a) load-deflection response of the girders, and (b) load-strain response in the stirrups.

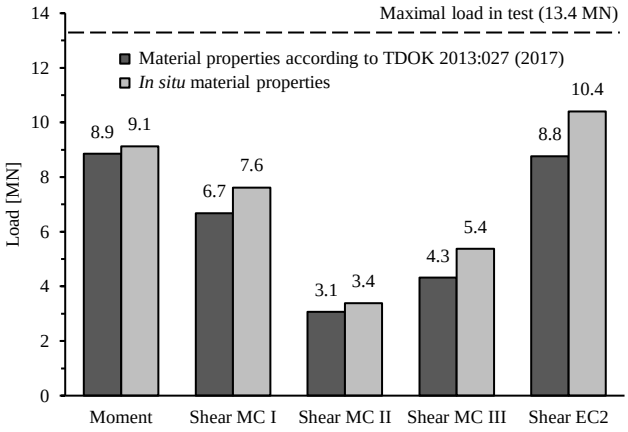

Figure 11. Load-carrying capacity with respect to moment and shear, using different resistance models, for material characteristics given by the assessment code and from the *in situ* tests.

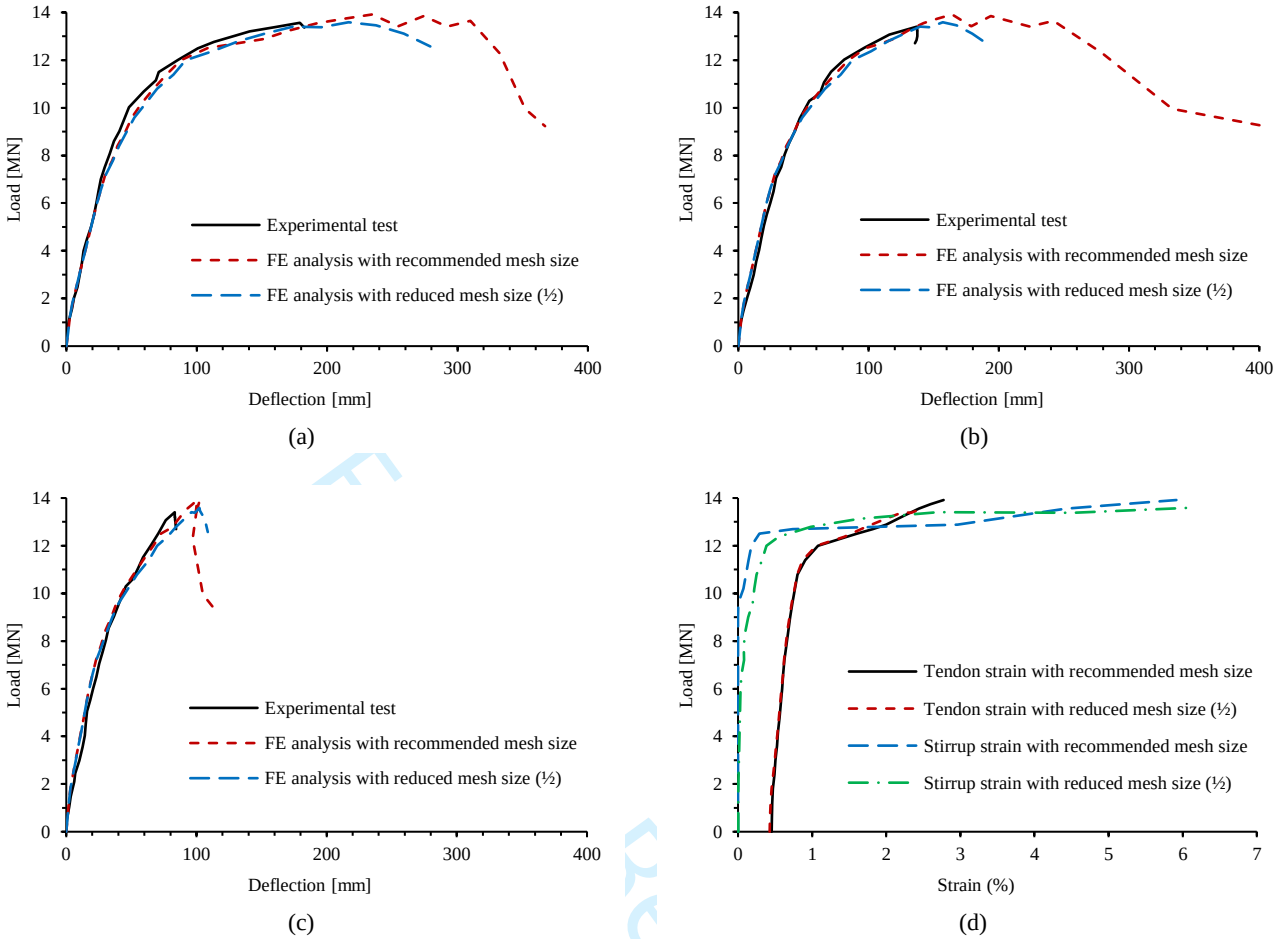

Figure 12. Bridge response according to nonlinear FE analysis based on the modelling framework: (a) load-deflection curves of south girder, (b) load-deflection curves of central girder, (c) load-deflection curves of south girder, and (d) load-strain curve of the tendon and stirrup that experienced the highest strain at peak load.

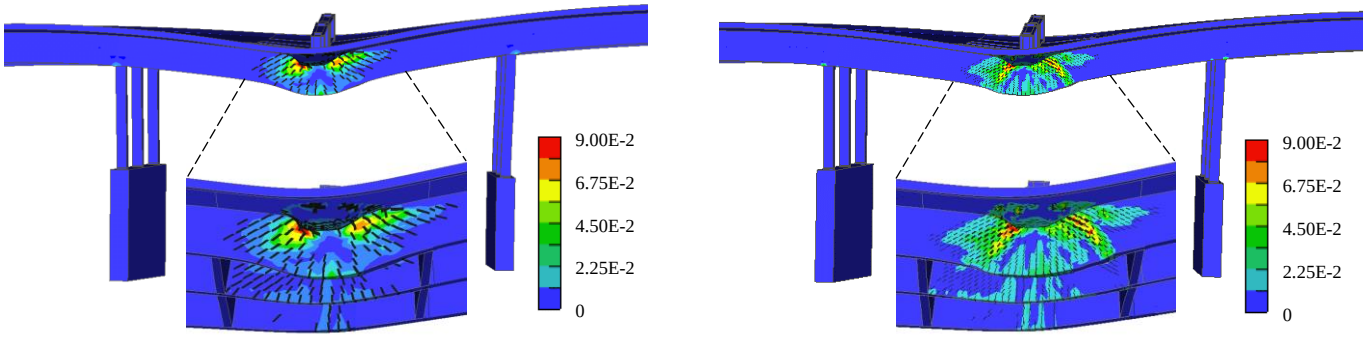

(a) (b)

Figure 13. Major principal concrete strains and concrete crack indications (≥ 2.0 mm) at the peak load predicted by nonlinear FE analysis: (a) analysis using the recommended size of finite elements, and (b) analysis using half the recommended size of finite elements (observe that the magnified detail show the girders from a lower view).